Check for updates

Colorimetric pH-responsive nanofibrous hydrogels for *in vitro* monitoring of wound infection

Nadia Banitorfi Hoveizavi, [a] Farzaneh Alihosseini,*[a] Sandro Lehner,[b] Philipp Meier[c] and Sabyasachi Gaan *[b]

Effective wound management is crucial for improving patient outcomes, particularly through timely detection of infections and monitoring of wound conditions. Addressing this critical need, this research develops nanofibrous hydrogels integrated with an indicator dye for real-time monitoring of wounds *via* a colorimetric method. A new double network nanofibrous hydrogels based on polyvinyl alcohol (PVA) and a phosphine oxide-based pH-sensitive hydrogel (namely PVA/Gel-A) with improved properties were produced through electrospinning. Their properties were examined through SEM, ICP-OES, FTIR, surface zeta potential, and mechanical analysis. Scanning electron microscopy and Brunauer–Emmett–Teller analysis confirmed the presence of smooth, bead free nanofibers with a mesoporous structure. The swelling ratio and surface zeta potential analysis further demonstrated the presence of anionic-cationic interpenetrating polymer networks (IPNs) in PVA/Gel-A compared to pristine PVA and Gel-A alone. Increasing the Gel-A content enhances moisture absorption in a dual system of PVA/Gel-A nanofibrous hydrogels. Compared to pristine PVA nanofibers, the PVA/Gel-A (1 : 1) nanofibers displayed enhancements in elastic modulus, tensile strength, and elongation of 216%, 154.5%, and 58%, respectively. It shows considerable strength while maintaining ductility, which is essential for flexible and durable applications. Then, the dye-doped PVA/Gel-A nanofibrous hydrogels, using bromothymol blue (BTB) as a pH-sensitive dye, were fabricated with and without a complexing agent. Their colorimetric and release behaviors were evaluated at different pH levels. The cationic complexing agent effectively prevented dye leaching, releasing less than 10% and ensuring chemical stability and accurate pH sensing. These IPNs can visibly indicate wound infections, resulting in the development of colorimetric nanofibrous hydrogels that monitor pH variations for smart wound dressing applications. *In vitro* cytotoxicity assessment applying keratinocytes demonstrates no toxic effects, underscoring their potential for safe clinical applications.

Introduction

Wound healing is a complex physiological process significantly influenced by various internal and external factors,[1–5] among which pH stands out as a crucial determinant.[6–9] The pH of a wound impacts essential functions such as oxygen release, angiogenesis, protease activity, and bacterial toxicity.[10] Healthy skin usually has a slightly acidic pH between 4 and 6, whereas chronic, non-healing wounds often have a pH above 7, indicating an increased risk of infection.[11] It is worth noting that the healing process is generally more efficient in an acidic environment, emphasizing the importance of pH regulation in wound management.[12]

Conventional wound dressings often struggle with problems such as inadequate moisture management, poor infection control, and limited adaptability to changing wound conditions.[13,14] This has led to an increased interest in advanced dressings that promote protection and healing and aid in the diagnosis of infection. Wound bed evaluations rely primarily on subjective assessments, with few practical diagnostic tools available for routine use. Monitoring surface pH could provide an objective measure of wound status, improve our understanding of healing responses, and aid the selection of more effective dressings.[13,15–18]

[a] Department of Textile Engineering, Isfahan University of Technology, Isfahan 84156-83111, Iran. E-mail: fhosseini@cc.iut.ac.ir

[b] Laboratory of Advanced Fibers, Empa, Swiss Federal Laboratories for Materials Science and Technology, Lerchenfeldstrasse 5, 9014 St. Gallen, Switzerland. E-mail: sabyasachi.gaan@empa.ch

[c] Laboratory of Nanomaterials in Health, Empa, Swiss Federal Laboratories for Materials Science and Technology, Lerchenfeldstrasse 5, 9014 St. Gallen, Switzerland

This journal is © The Royal Society of Chemistry 2025

J. Mater. Chem. B, 2025, **13**, 11621–11639 | 11621

In recent years, smart wound dressings have emerged as innovative solutions utilizing technology to improve healing.[19,20] These dressings respond to changes in the wound environment, providing real-time feedback and optimal healing conditions while reducing the frequency of painful dressing changes. Technologies such as electrochemical and colorimetric methods facilitate real-time monitoring of key wound parameters, including pH, temperature, and oxygen levels.[13,17,21–23] One approach within the colorimetric method involves the use of pH-sensitive dyes.[24–26] A key feature of these colorimetric smart dressings is their color change in response to environmental changes, indicating wound healing status and signaling the potential onset of infection. This real-time monitoring provides healthcare professionals with crucial information about treatment effectiveness and wound progression, enabling timely adjustments to care.[26] Overall, these smart dressings provide a non-invasive and convenient way to monitor healing and improve patient outcomes.[27]

Bromothymol blue (BTB) is a highly effective pH indicator among the various materials used in these dressings. Its ability to turn from yellow to blue in an acidic environment and take on a green tint at neutral pH makes it invaluable for laboratory applications such as titrations and biochemical analysis. In addition, BTB is used in medical diagnostics to detect diseases such as urinary tract infections[28] and in biological studies[29] to trace fluid movements and visualize cell structures. Its non-toxic properties and clear color transitions make it a reliable tool in education and research.

Another critical factor in the utilization of dyes is the prevention of leaching. To address this issue, various methods have been employed to incorporate dyes, including the physical blending of dyes with precursor materials or the covalent attachment of dyes to polymer chains during hydrogel synthesis.[30,31] Various approaches have been used to stabilize BTB dyes on substrates. In one study, BTB was grafted onto cellulose modified with hydroxypropyltriethylamine groups to obtain pH-sensitive fibers[32] and films.[33] In another case, a polyamine-based resin has been utilized as a dye-fixing agent for cotton fibers.[34] Brooker et al. integrated BTB into a collagen-based wound dressing for real-time infection detection by color change, demonstrating that the drop-cast method significantly enhanced BTB retention and durability compared to electrospinning techniques.[30]

Nanofibrous hydrogels have gained considerable attention for applications in wound healing, tissue engineering, and drug delivery due to their unique properties.[35–38] These hydrogels are composed of semi- and fully interpenetrating polymer networks (IPNs), which include conventional polymers such as vinyl polymers, polyurethanes, and polyacrylates. Their three-dimensional, crosslinked structures can absorb and retain large amounts of water, creating a moist environment that promotes wound healing. Additionally, their biocompatibility and soft and flexible nature make them ideal for wound dressings.[39–43] Meanwhile, nanofibers' high surface area, porosity, and mechanical strength increase their effectiveness in wound care by improving cell adhesion and responsiveness to biochemical signals. For example, Rybak et al. developed a 3D-printed hydrogel for infected wounds, featuring DMX-loaded electrospun mats with gold nanorods (AuNRs) in short filaments (SFs) embedded in a GelMA/SA scaffold. NIR light triggers controlled DMX release, with strong photothermal, antibacterial, and biocompatibility properties.[44]

Among the various polymers used in nanofibrous hydrogels, polyvinyl alcohol (PVA) stands out due to its favorable biocompatibility, biodegradability, and mechanical properties, making it a significant choice for the development of these advanced materials.[45,46]

Cationic hydrogels, characterized by their hydrophilic polymer networks embedded with positively charged groups, have shown great potential within biomedical applications.[47] These hydrogels interact with negatively charged molecules and surfaces and exhibit remarkable pH sensitivity and the ability to form complexes with anionic substances. This makes them ideal for drug delivery, gene therapy, and environmental remediation. Recent studies have highlighted their effectiveness in targeted drug delivery, particularly for anticancer treatments, due to their ability to release drugs in response to specific stimuli.[11,48] Additionally, cationic hydrogels have demonstrated significant efficacy in adsorbing toxic ions, making them valuable for removing heavy metals from wastewater. Their inherent versatility and reactivity continue to drive research into their various biomedical and environmental applications.[49,50]

This study explores the development of innovative smart wound dressings based on hybrid dual-network nanofibrous hydrogels, combining PVA and a phosphate-containing cationic hydrogel (Gel-A). While pH-responsive hydrogel systems have been extensively studied, the number of reported cationic hydrogels remains limited, particularly in the context of nanofibrous IPNs for wound care. Building on our previous work that introduced Gel-A, a transparent, pH-sensitive, and biocompatible hydrogel synthesized via a one-step Michael addition reaction, we address its major limitation: inadequate mechanical strength. In this work, we integrate Gel-A with mechanically robust PVA using a green, citric-acid-mediated crosslinking strategy coupled with thermal treatment, forming a full-IPN nanofibrous architecture that provides both structural stability and functional responsiveness. Notably, this system presents an anionic–cationic balance within the matrix, promoting electrostatic interaction and enhancing dye retention.

To our knowledge, this is the first report combining a phosphine-oxide-based cationic hydrogel, PVA, and the colorimetric dye BTB into an electrospun IPN nanofiber platform for wound monitoring. Electrospinning, rarely applied to such IPN hydrogel systems, confers a high surface-to-volume ratio, significantly improving the rate and sensitivity of pH detection. Moreover, BTB was effectively immobilized within the nanofiber network using a cationic complexing agent, preventing leaching and preserving its colorimetric integrity over time, an essential feature for wound safety and long-term functionality. The resulting nanofibrous dressing not only enables real-time, visible pH-based infection monitoring but also serves as a mechanically durable and biocompatible platform, with strong potential for clinical translation. This novel material design

11622 | J. Mater. Chem. B, 2025, **13**, 11621–11639

This journal is © The Royal Society of Chemistry 2025

represents a significant advancement in the development of responsive, non-invasive wound care technologies.

Experimental

Materials

PVA (Mn = 125 000 g mol^{-1}) was supplied from Aldrich. Phosphorus(V) oxychloride, vinylmagnesium bromide solution 1.0 M in THF, tetrahydrofuran anhydrous, dichloromethane, ammonium chloride, heptane, citric acid (CA), and piperazine (PP) were purchased from Sigma-Aldrich. Trivinylphosphine oxide (TVPO) was synthesized like the previous study with some modifications.[51]

BTB was obtained from Merck. Poly (diallyldimethylammonium chloride) (PDADMAC) (20 wt% solution in water, average M_w = 200 000–350 000 g mol^{-1}, density = 1.04 g mL^{-1}) was provided from Sigma-Aldrich. Buffer solutions with varying pH levels were supplied by Honeywell Fluka™ (Germany).

Electrospinning procedure

Fabrication of PVA nanofiber. To fabricate PVA nanofibers, PVA powder was slowly added to deionized water at room temperature and then stirred at 80 °C for 2 hours by a magnetic stirrer to obtain a clear and homogeneous solution with a concentration of 8% w/w. Then, it was allowed to be cool to room temperature and stirred overnight. Citric acid as a green crosslinking agent was then added to the solution at 0.48 wt% to the weight of the solution under stirring for half an hour. To ensure a homogeneous solution, the prepared solutions were sonicated for 10 minutes before electrospinning.

Electrospinning of all solutions was performed at a temperature of 25 °C and relative humidity of around 35–50%. The well-mixed solution was poured into the syringe and pumped through a syringe pump at a flow rate of 0.3 mL h^{-1}. The needle of the syringe was connected to the positive electrode of the high-voltage power supply, and electrospinning was performed at 15 kV (applied voltage) and a working distance of 16 cm (the tip of the needle to the collector distance) based on the preliminary results. The electrospun nanofibers mats were collected on a rotating collector with a speed of around 260 rpm wrapped with aluminum foil. After electrospinning, the prepared electrospun mat was heat-treated for 1 h at 130 °C, obtaining a cross-linked network of PVA nanofibrous hydrogel. It is worth to note that owing to the dissolution of non-crosslinked PVA nanofiber in water, cross-linking with citric acid and post-heat treatment at 130 °C improves its effectiveness.[52] PVA nanofibers without citric acid and post-heat treatment were also produced for comparison.

Fabrication of PVA/Gel-A nanofibrous hydrogel. For this purpose, a PVA solution with a concentration of 8% w/w was prepared as mentioned above and stirred overnight, followed by adding PP and TVPO (with a molar ratio of 1.5:1) at 25%, 50%, 100%, and 150% w/w (with regard to the weight of PVA) and stirred at room temperature for another half an hour to form a homogeneous solution. Then citric acid with a

concentration of 0.48% w/w (to the weight of the solution) was added and continuously stirred for another half an hour. The remainder of the process follows the same procedures for fabricating PVA nanofibers. After electrospinning, the resulting nanofiber mats were heat-treated at 130 °C for one hour. This treatment aimed to create a dual cross-linked network, which includes Gel-A containing TVPO and PP, along with a cross-linked network of PVA. This process results in the formation of the PVA/Gel-A nanofibrous hydrogel. Fig. 1 illustrates a schematic representation of the preparation of the PVA/Gel-A nanofibrous hydrogel.

Additionally, the viscosity and conductivity of PVA and PVA/Gel-A (1:1) solutions were measured using a Brookfield viscometer (USA) with spindle 18 at 5 rpm and a Prisma Tech conductivity meter (Iran) at room temperature, respectively.

Fabrication of the colorimetric substrate. Smart calorimetric nanofibers were fabricated via a dye-doped electrospinning method. A PVA + PP and TVPO (PVA/Gel-A) blend solution, prepared with a 1:1 weight ratio, served as the polymer matrix. The electrospinning parameters and procedure were consistent with those previously optimized in our laboratory for PVA/Gel-A (1:1) nanofibers. To impart pH sensitivity, BTB was incorporated into the aforementioned polymer solution at a concentration of 2.5% w/w relative to the total polymer weight prior to electrospinning. This sample is designated PVA/Gel-A/BTB. Furthermore, to mitigate potential BTB leaching, a separate sample, designated PVA/Gel-A/BTB/PDADMAC, was prepared. This involved the addition of PDADMAC at a concentration of 6% w/w relative to the total polymer weight to the PVA/Gel-A (1:1) solution already containing BTB at 2.5% w/w relative to the total polymer weight, prior to electrospinning. Following electrospinning, both resulting nanofiber mats were subjected to a heat treatment at 130 °C for one hour to enhance cross-linking.

Characterization

Scanning electron microscope (SEM). The surface morphology of the nanofibrous hydrogel samples was examined using a Hitachi S-4800 scanning electron microscope (Tokyo, Japan) at an accelerating voltage of 2 kV at a working distance of 8 mm. Before measuring, a piece of the nanofiber samples was cut and placed on a special holder containing double-sided carbon glue. Then, the samples were sputter-coated with a thin layer of gold and palladium (Leica) under an argon atmosphere with a thickness of 8 nm for nanofiber. To determine the diameter of nanofibers, the diameter of 100–200 different individual nanofibers was measured using Digimizer software, and the average diameter of nanofibers and standard deviation were reported.

The phosphorus content of the nanofibers was measured using the inductively coupled plasma optical emission spectroscopy method (ICP-OES) on a 5110 ICP-OES (Agilent Switzerland AG, Basel, Switzerland) apparatus under an argon plasma. Sample preparation for ICP-OES consisted of mixing 100 mg of a sample with 3 mL HNO$_3$, followed by digestion using an MLS-MWS turboWAVE INERT microwave reactor (Germany). The digestion process was done at 250 °C for 50 minutes. After digestion,
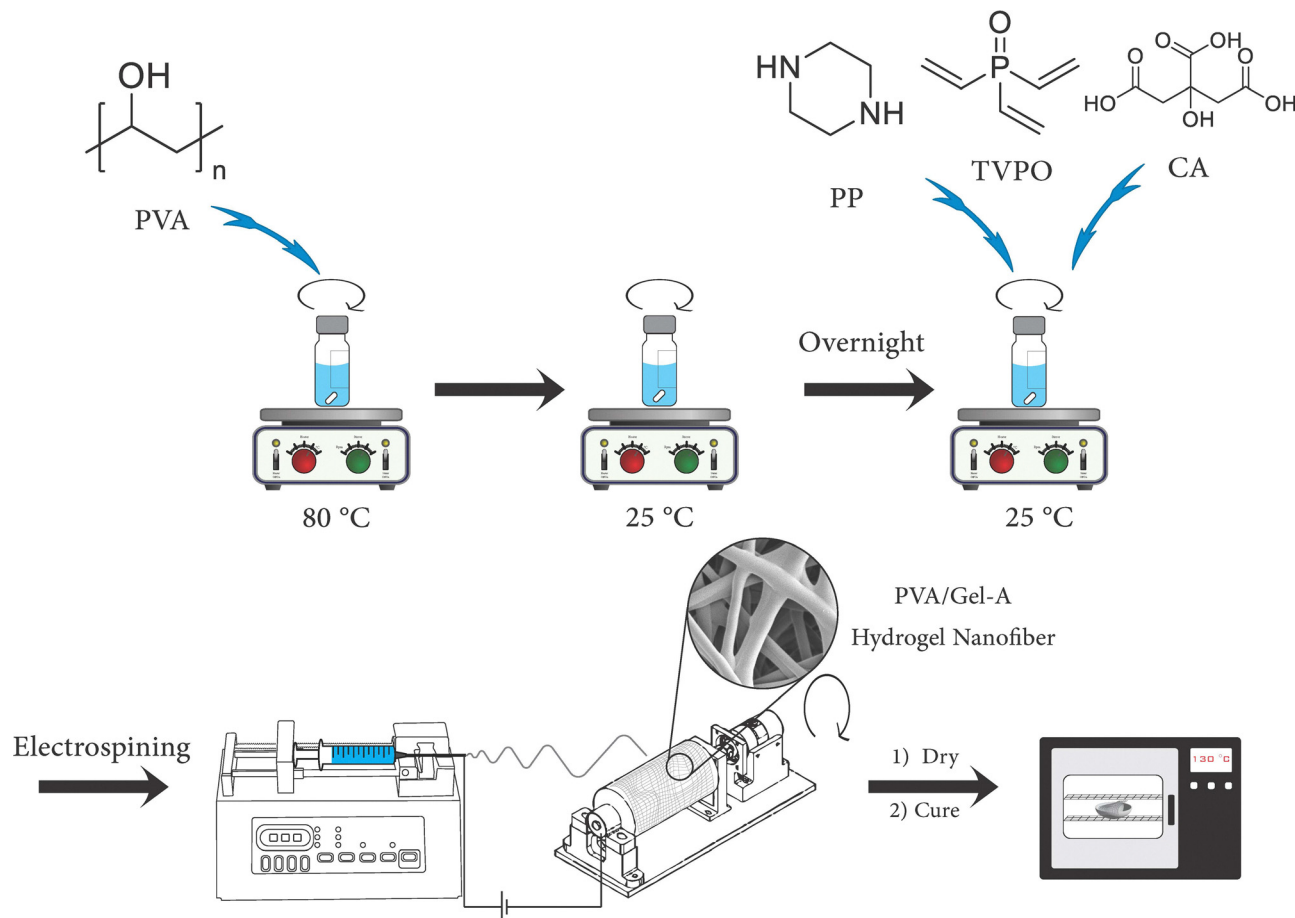
Fig. 1 Schematic depicting the electrospinning process for fabricating PVA/Gel-A nanofibrous hydrogels.

at least four dilution standard solutions with known concentrations were prepared from the main standard solution, CGP1, which contains 999 ± 4 µg mL^{-1} phosphorus in H_2O (Inorganic Ventures). A 2% v/v nitric acid solution was used as a control solution for dilution. The calibration curve was then plotted using ICP-Expert software, considering the two emission wavelengths of the phosphorus element, 213.618 nm and 214.914 nm.

Brunauer–Emmett–Teller (BET) analysis was performed on BELSORP-miniX (Microtrac MRB). The surface area and average pore size were determined using the BET method, with the total pore volume calculated at a relative pressure of $P/P_0 = 0.990$, and adsorption and desorption isotherms obtained at a relative pressure (P/P_0) of up to ~ 0.990 at 77 K.

Mechanical properties of the nanofibers were evaluated using a Zwick & Roell Tensile Tester (Germany), with three replicates conducted for each sample. The thickness of the nanofiber samples was measured using a digital micrometer (Digital Outside Micrometer, 3109-25B, INSIZE, China) at 10 different points to ensure accurate calculations of stress during tensile testing. Prior to the analysis, the samples were conditioned at a relative humidity of $50 \pm 2\%$ and a temperature of 23 °C for 48 hours. Each sample was cut to dimensions of 5×30 mm^2, and the tensile tests were performed at 25 °C with

a cross-head speed of 2 mm min^{-1} and an initial grip separation of 18 mm to assess the mechanical properties of the nanofibers.

Surface zeta potential measurements were performed on an Anton Paar SurPASS 3 (Austria) to characterize the surface charge of PVA, and PVA/Gel-A nanofibrous hydrogels using SurPASS^{TM} 3 adjustable gap cell as a measuring cell. The surface zeta potential was measured as a function of pH in the range from 3 to 10 increasing with a step of 0.3 ($n = 4$ in each step) over time until the final pH reaches 10.

$$\text{Swelling ratio}\% = \frac{W_t - W_0}{W_0} \times 100 \qquad (1)$$

The swelling ratio was determined by cutting small specimens of nanofibrous hydrogels and weighing them both before (W_0) and after soaking (W_t) in various buffer solutions (i.e., pH 2, 4, 7, and 9) at 25 °C for 24 hours. After soaking, excess solvent was carefully removed from the surface using a moist tissue. The swelling ratio percentage was subsequently calculated using the following equation.

Fourier-transform infrared (FTIR) spectra of the nanofibers were recorded using a Bruker Tensor 27 FTIR spectrometer (Bruker Optics, Ettlingen, Germany) over the wavenumber

11624 | J. Mater. Chem. B, 2025, **13**, 11621–11639

This journal is © The Royal Society of Chemistry 2025

range of 4000 to 600 cm^{-1}, employing 32 scans at a resolution of 4 cm^{-1}.

Cytotoxicity of nanofibrous hydrogels

KeratinoSens assay. The *in vitro* cytotoxicity of Gel-A, PVA and PVA/Gel-A nanofibrous hydrogels was assessed by applying a KeratinoSens skin irritation and sensitization assay according to OECD test guideline 442D.[53] KeratinoSens® human kerati-nocyte cells (instaCELL® KeratinoSens®, acCELLerate GmbH, Germany) were cultured in DMEM (Sigma-Aldrich, Switzerland) supplemented with 10% fetal bovine serum, 1% L-glutamine, and 500 μg mL^{-1} G418. Cells (passages P6-P25) were seeded at 10 000 cells per well in 96-well plates (Techno Plastic Products, Switzerland) and adapted to G418-free medium for 24 hours at 37 °C and 5% CO$_2$.

Hydrogels and nanofibers were sterilized in PBS and stirred overnight. The extraction procedure followed ISO-10993-12 guidelines,[54] using 0.2 g mL^{-1} for hydrogels and 0.1 g mL^{-1} for nanofibers in artificial sweat solution, incubated for 24 hours at 37 °C. Extracts were diluted to final concentrations of 10%, 5%, 2.5%, and 1.25% in DMEM containing 1% DMSO.

Cells were exposed to these sample extracts additionally DMEM containing 0.5–1000 μM EGDMA served as assay internal positive control assuring the accuracy of each KeratinoSens assay. Each condition was tested in triplicate ($N = 3$, $n = 3$).

Cell viability assay. Cell viability was assessed by applying an Alamar Blue assay (ThermoFisher Scientific, Switzerland). Keratinocyte cells were exposed for 48 hours to four above-mentioned concentrations of hydrogel and nanofiber sub-stances. After exposure, the supernatant was first discarded and cells were washed twice with PBS prior to replacement with fresh medium containing 10% v/v alamarBlue solution. Cells were incubated for 3 hours at standard cell culture conditions at 37 °C and 5% CO$_2$. Fluorescence intensity was measured using a Mithras LB 943 Plate Reader (Berthold Technologies, Germany) with MikroWin software at excitation and emission wavelengths of 540 nm and 590 nm, respectively.

Sensitizing effect quantification. Sensitizing behavior was quantified using the One-Glo™ Luciferase assay (Promega, USA). A solution of 1:1 PBS and One-Glo™ Luciferase (100 μL) was added to keratinocytes, followed by a 20-minute incubation at room temperature in darkness. Subsequently, luminescence intensity was measured using a Synergy H1 microplate reader (BioTek, USA) and normalized.

In vitro experiments were conducted with three independent extractions and three technical triplicates per condition in five independent experiments for both Alamar Blue and One-Glo™ Luciferase assays. Standard deviations were calculated. Assay validity was confirmed by an assay internal positive controls (EGDMA; sensitization EC$_{1.5}$: 5–125 μmol; irritation IC$_{50}$: >500 μmol) and negative controls (medium with and without cells). Endpoint values evaluated included Imax (maximal average fold induction of luciferase activity), EC$_{1.5}$ (concen-tration for >1.5-fold luciferase expression increase), and IC$_{30}$ and IC$_{50}$ (concentrations for 30% and 50% cell viability reduction, respectively).[53]

UV-visible absorption spectra. BTB solution (132 ppm) were diluted (1:10) using the corresponding buffer solutions at different pH values ranging from 4 to 9. The UV-vis absorption spectra of these solutions were recorded from 300 to 700 nm (Shimadzu, UV-mini1240, Japan).

Dye release study. To study dye release, two calibration curves were established at the absorbance maxima (λ_{max}) of 434 nm and 616 nm, corresponding to pH 5 and 8, respectively. Nanofiber samples were cut, weighed, and placed in test tubes with 1 mL of each buffer solution (pH 5 and 8). At various time intervals, samples were transferred to new test tubes containing 1 mL of fresh buffer solution. The absorbance of each solution at the corresponding maximum wavelength was measured and converted to concentration using the equations obtained from the calibration curves. The percentage of dye release was then calculated as eqn (2).

$$\%\text{Release} = \frac{M_t}{M_0} \times 100 \tag{2}$$

where M_t represents the mass of BTB released at time t, and M_0 represents the initial mass of BTB incorporated within the nanofiber sample.

Colorimetry. The reflectance values of the halochromic dressings were measured using a Spectraflash spectropho-to-meter (Datacolor, Switzerland) under illuminant D65 using 10° standard observers. Color strength (K/S) values of each sample were calculated from the reflectance values using the well-known Kubelka–Mank method (eqn (3)).[55]

$$\frac{K}{S} = \frac{(1 - R)^2}{2R} \tag{3}$$

where K is the absorption coefficient, S is the scattering coefficient and R is the reflectance at complete opacity.[55] The color parameters ($L\star$, $a\star$, $b\star$, $C\star$, $h°$) were also determined where $L\star$ = lightness; $a\star$ = greenness/redness; and, $b\star$ = blueness/yellowness, $C\star$ = chroma and $h°$ = hue angle.[56] A standard white screen background was utilized, with color coordinates of $L\star = 92.92$, $a\star = 2.95$, and $b\star = -7.58$. This background was placed behind each nanofiber sample to ensure opacity. All analyses were carried out in three replicates.

Results and discussions

The principle of full-IPNs PVA/Gel-A nanofibrous hydrogels formation

This study introduces the production of nanofibrous hydro-gels with a unique IPN structure, integrating PVA and Gel-A (phosphine oxide-based cationic hydrogel).

In a previous study, a transparent, cationic pH-responsive Gel-A was synthesized from the reaction between PP and TVPO *via in situ* Michael addition reaction, without the need for any initiators or crosslinkers.[51] This study aims to use PP and TVPO along with PVA to fabricate full-IPN nanofibrous hydrogels. From a synthetic perspective, the synthesis of the two networks in the IPNs can occur either sequentially or simultaneously (*in situ*). In sequential IPNs, one network swells while the other
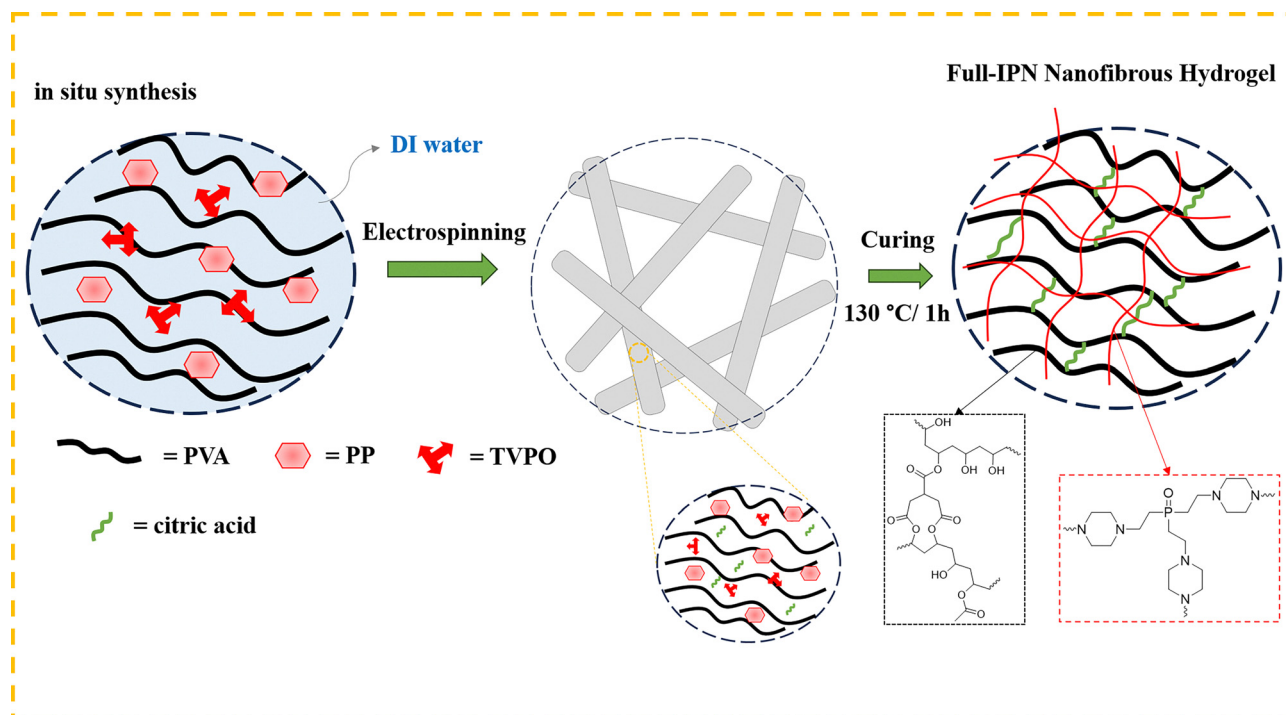
This journal is © The Royal Society of Chemistry 2025

J. Mater. Chem. B, 2025, **13**, 11621–11639 | **11625**

Fig. 2 Proposed mechanism for the formation of interpenetrating polymer network structure within PVA/Gel-A nanofibrous hydrogels.

polymerizes in its presence. In simultaneous IPNs, all reactants are combined prior to the initiation of any polymerization or cross-linking reactions. Additionally, both network precursors are synthesized independently and concurrently, without any interference.[57,58] Therefore, the mechanisms leading to the formation of each network must differ to avoid the formation of a single copolymer network through undesired cross-reactions. Often, these reactions result in a synergistic enhancement of properties compared to those of the individual polymer components.[59,60] As can be seen from Fig. 2, this study utilized a simultaneous methodology followed by a curing process, wherein PVA was crosslinked with citric acid. At the same time, PP acted as a Michael donor and trivinylphosphine oxide served as a Michael acceptor. This arrangement facilitated the *in situ* formation of phosphine oxide polymeric networks physically entrapped within the PVA matrix. Therefore, after the post-heat treatment at 130 °C, a robust double-crosslinked network was achieved, comprising the PVA framework and Gel-A. The precise structure of the cross-linked PVA/Gel-A nanofibers is uncertain; however, it can be considered a two-component system comprising cross-linked Gel-A networks within a cross-linked PVA matrix, forming a so-called full-IPN. A similar principle has previously been demonstrated in the *in situ* phosphine oxide flame retardant networks treatments for cotton cellulose,[61] nanoscale hybrid polyaniline/cationic Hydrogel/poly(ε-caprolactone) for the highly efficient catalytic conversion of cellulose,[62] and *in situ* flame retardant macromolecules in polyamide 6.[63]

As mentioned earlier, this study investigates the synergistic effects of PVA and cationic phosphate-based hydrogels,
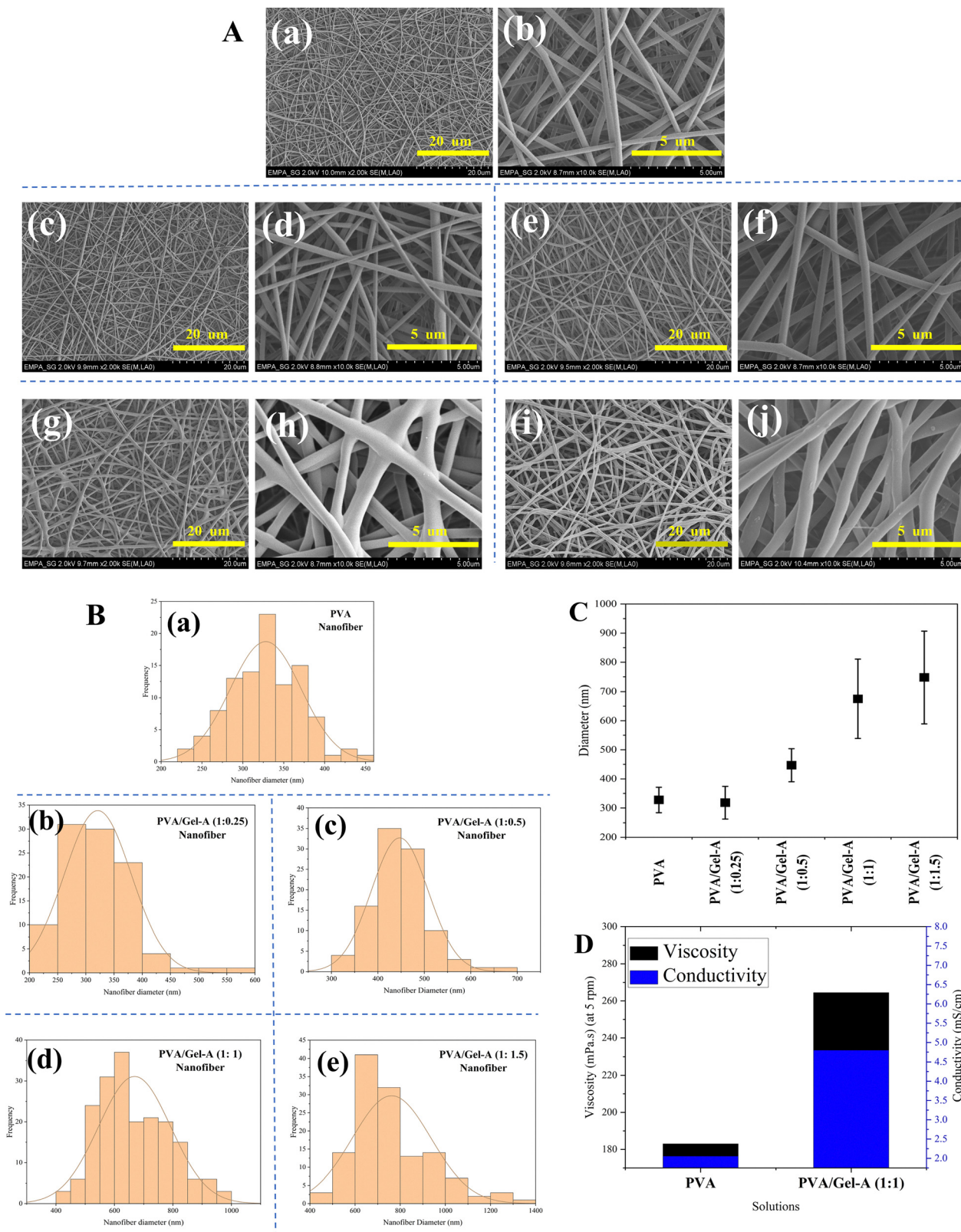
alongside the integration of BTB as a pH indicator, to contribute to the advancement of wound care technologies. The following sections aim to enhance the understanding of how chemical composition influences the functionality of advanced hydrogel systems.

Surface morphology of PVA and PVA/Gel-A nanofibrous hydrogels

The surface microscopic morphology of the electrospun nanofibers was examined using scanning electron microscopy with two magnitudes of ×2.0k and ×10.0k, respectively. Fig. 3A and B show SEM images of the PVA/Gel-A nanofibrous hydrogels together with the corresponding size distribution histograms, respectively.

Scanning electron microscopy (SEM) revealed that electrospun PVA nanofibers (Fig. 3A(a and b)) exhibited a smooth, bead-free morphology with a narrow diameter distribution. The average fiber diameter was 328 ± 44 nm. Incorporation of Gel-A into the PVA solution, at Gel-A to PVA weight ratios of $0.25:1$, $0.5:1$, $1:1$, and $1.5:1$, also resulted in smooth, bead-free nanofibers with random orientations (Fig. 3A(c–j)). Quantitative analysis of fiber diameters (Fig. 3B and C) demonstrated a progressive increase in average fiber diameter with increasing Gel-A content. Fig. 3C illustrates the average nanofiber diameter $\pm$ standard deviation for each PVA/Gel-A composition. The data reveals that the average fiber diameter varies with the PVA/Gel-A ratio, but in all cases remains below 750 nm. Specifically, the average diameter increased from 319 ± 56 nm for PVA/Gel-A $(1:0.25)$ to 748 ± 159 nm for PVA/Gel-A $(1:1.5)$. This indicates that the addition of Gel-A leads to the formation of thicker and less uniform nanofibers compared to pure PVA.

11626 | *J. Mater. Chem. B*, 2025, **13**, 11621–11639

This journal is © The Royal Society of Chemistry 2025

Fig. 3 (A) Scanning electron micrographs of PVA/Gel-A nanofibers at varying weight ratios: (a) and (b) pure PVA, (c and d) PVA/Gel-A (1 : 0.25), (e and f) PVA/Gel-A (1 : 0.5), (g and h) PVA/Gel-A (1 : 1), (i) and (j) PVA/Gel-A (1 : 1.5). Scale bars: 20 μm (left) and 5 μm (right). (B) Nanofiber diameter distributions for: (a) pure PVA, (b) PVA/Gel-A (1 : 0.25), (c) PVA/Gel-A (1 : 0.5), (d) PVA/Gel-A (1 : 1), and (e) PVA/Gel-A (1 : 1.5). Distributions were determined from SEM images (n = 100–200). (C) Average diameter of nanofibrous hydrogels fabricated. (D) Viscosity and conductivity of pure PVA and PVA/Gel-A (1 : 1) solutions prior to electrospinning.

This journal is © The Royal Society of Chemistry 2025

J. Mater. Chem. B, 2025, **13**, 11621–11639 | **11627**

The observed increase in fiber diameter with increasing Gel-A content can be attributed to changes in the electrospinning solution's properties. Furthermore, the addition of PP and TVPO, intended to induce crosslinking within the nanofibers, may also influence fiber morphology. Measurements of solution viscosity and conductivity (Fig. 3D) showed that the addition of Gel-A to PVA resulted in increased viscosity and conductivity. The viscosity of the PVA/Gel-A (1 : 1) solution was significantly higher (264.5 mPa s) than that of the pure PVA solution (183 mPa s). Similarly, the conductivity of the PVA/Gel-A (1 : 1) solution (4.8 mS cm^{-1}) was approximately 2.3 times greater than that of the pure PVA solution (2.1 mS cm^{-1}). The higher viscosity, arising from increased chain entanglement, leads to greater viscoelastic forces that resist the electrostatic stretching force during electrospinning, potentially resulting in thicker fibers.[64–66] Increased conductivity also influences fiber formation; a higher charge density on the electrospinning jet, resulting from increased conductivity, typically leads to greater stretching and a reduction in fiber diameter.[66–69] However, in this system, despite the increase in conductivity with increasing Gel-A content, the observed increase in fiber diameter suggests that the effect of viscosity is more pronounced. It is possible that the increased viscosity dampens the effect of the increased charge density, or that the relationship between conductivity and fiber diameter is not linear in this particular system. Hence, it is plausible that PP and TVPO could alter the effective molecular entanglement and interchain interactions within the polymer solution, further influencing the spinnability and leading to the observed diameter changes. However, further investigation is needed to fully elucidate the specific effects of PP and TVPO on the electrospinning process and the resulting nanofiber morphology.

Inductively coupled plasma - optical emission spectrometry (ICP-OES) analysis (Table 1) confirmed the presence of phosphorus in the nanofibrous hydrogel samples. The measured phosphorus content was in good agreement with the theoretically calculated values based on the hydrogel composition, indicating efficient incorporation of phosphorus-containing components within the nanofiber matrix.

FTIR of Gel-A, PVA, and PVA/Gel-A nanofibrous hydrogels

The FTIR spectrum of Gel-A, PVA, and PVA/Gel-A nanofibrous hydrogels produced in a single step with different proportions of Gel-A (1 : 0.25, 1 : 0.5, 1 : 1, and 1 : 1.5) is shown in Fig. 4.

Table 1 Quantitative analysis of phosphorous in nanofibrous hydrogels by ICP-OES, compared to theoretical phosphorous content based on hydrogel composition

Substrate	Phosphorous amount	
	ICP-OES	Calculated
PVA	—	—
PVA/Gel-A (1 : 0.25)	2.11	2.36
PVA/Gel-A (1 : 0.5)	3.46	3.94
PVA/Gel-A (1 : 1)	4.73	5.91
PVA/Gel-A (1 : 1.5)	6.10	7.09

In the case of the PVA nanofiber, the peaks at 1210 cm^{-1} to 1236 cm^{-1} correspond to the linear vibrations of ether –COO bond, emphasizing the formation of ester bonds. The peaks of 1094 cm^{-1} and 1141 cm^{-1} are respectively associated with the stretching vibrations of the –C–O and –C–OH groups. However, some researchers also attribute the 1141 cm^{-1} peak to the stretching vibrations of the C–C bond in the polymer chain in the crystalline part. In addition, the carbonyl peak at 1725 cm^{-1} is related to the ester groups formed by the chemical interactions between hydroxyl groups of PVA and carboxyl groups of citric acid.[68,70,71] C–H bending absorption was represented at 1465 cm^{-1}, and symmetric and asymmetric stretching vibrations of C–H appeared at 2819 cm^{-1} and 2940 cm^{-1}, respectively. These results are in well agreement with other literature.[72,73] In the case of PVA/Gel-A nanofibers, the stretching vibrations of –P=O appeared at 1125 cm^{-1} and –C–P=O at about 998 cm^{-1}. C–N bending vibrations appeared at 1354 cm^{-1} and the peak was observed at 1577 cm^{-1}, related to the end –NH groups of Gel-A. As the Gel-A content in the PVA/Gel-A nanofibers increases, the intensity of peaks at 1654, 1577, 1276, 1125, and 998 cm^{-1} become more pronounced. This indicates that the Gel-A network forms *via* a Michael reaction between PP and TVPO in the PVA/Gel-A system. A broad peak at 3330 cm^{-1} is associated with the stretching vibrations of the –OH bond from the intermolecular and intramolecular hydrogen bonds in the moisture absorbed by the nanofibrous hydrogels. Additionally, the peak at 1654 cm^{-1} corresponds to entrapped water molecules in the hydrogels, attributed to the bending vibration of the O–H bond, indicating their presence in the hydrogel matrix. It can be seen from Fig. 4 that the PVA/Gel-A FTIR spectra have both an absorption peak of PVA and an absorption peak of Gel-A, indicating that the addition of PP and TVPO to PVA nanofibers did not lead to the formation of a new bond because no new peak was observed in the IR spectrum compared to the spectrum of Gel-A and PVA hydrogels.

BET analysis

The physical properties of prepared nanofibrous hydrogels *e.g.*, pure PVA and PVA/Gel-A (1 : 1) in terms of specific surface area, pore volume and pore diameter were measured by nitrogen adsorption/desorption method. The notable decrease in surface area (from 10.3 m^2 g^{-1} for PVA to 2.52 m^2 g^{-1} for PVA/Gel-A) further suggests a transition to a more densely packed structure rather than a loose one. It should be noted that the diameter of nanofibers significantly influences their specific surface area, with smaller diameters leading to larger surface areas.[74] This study similarly demonstrates that PVA/Gel-A nanofibers possess a greater diameter (674 nm) and, consequently, a lower surface area compared to pure PVA nanofibers, which have a diameter of 327 nm. Additionally, a significant reduction in total pore volume (from 0.027 cm^3 g^{-1} for PVA to 0.007 cm^3 g^{-1} for PVA/Gel-A) indicates that the amount of void space within the material decreases with the addition of Gel-A, suggesting a denser packing of the polymer chains, which enhances the structural stability.[75,76] The similar

11628 | *J. Mater. Chem. B*, 2025, **13**, 11621–11639

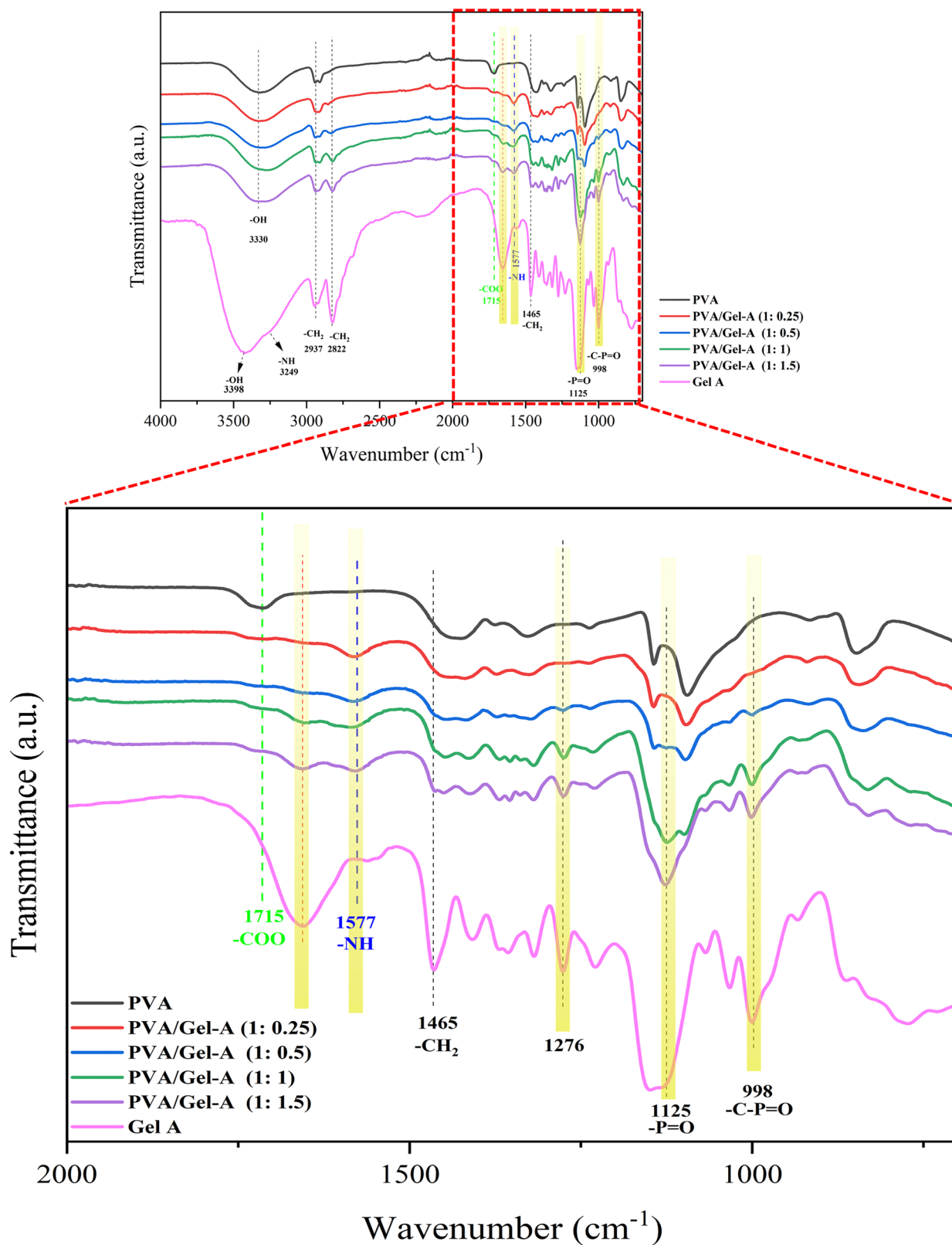This journal is © The Royal Society of Chemistry 2025

Fig. 4 Fourier transform infrared (FTIR) spectra of Gel-A, pure PVA, and PVA/Gel-A nanofibrous hydrogels at varying weight ratios, showing characteristic functional groups (600–4000 cm^{-1}). The inset displays the expanded region from 600 to 2000 cm^{-1}.

average pore diameter (10.79 nm for PVA and 10.75 nm for PVA/Gel-A) indicates that the addition of Gel-A does not significantly alter the size of the pores, suggesting that the basic pore structure remains stable.
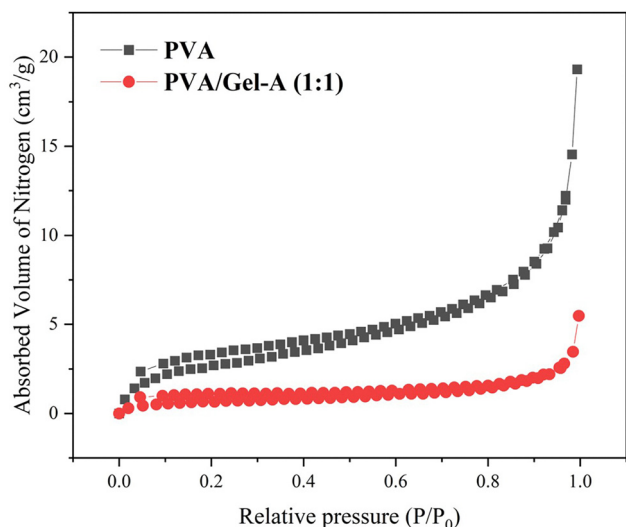
This journal is © The Royal Society of Chemistry 2025

J. Mater. Chem. B, 2025, **13**, 11621–11639 | **11629**

Fig. 5 Nitrogen adsorption/desorption isotherms for pure PVA and PVA/Gel-A (1:1) nanofibers.

Table 2 Summary of surface area and porosity parameters for pure PVA and PVA/Gel-A (1:1) nanofibers, as determined by Brunauer–Emmett–Teller (BET) analysis

Samples	Surface area ($m^2 g^{-1}$)	Total pore volume ($cm^3 g^{-1}$)	Average pore diameter (nm)	Structure	Isotherm
PVA	10.30	0.027	10.79	Mesoporous	IV
PVA/Gel-A (1:1)	2.52	0.007	10.75	Microporous	IV

Table 3 Compressive mechanical properties of Gel-A: stress (kPa), strain (%), and modulus (kPa). Results are presented as mean ± standard deviation ($n = 3$)

Sample	Compression stress (kPa)	Compression strain (%)	Compression modulus (kPa)
Gel-A	11± 4	57.24 ± 6.39	0.1921

Moreover, according to the IUPAC classification, porous structures can contain pores smaller than 2 nm, between 2 and 50 nm, and larger than 50 nm, and form microporous, mesoporous, and macroporous structures, respectively.[77] Based on the BET analysis data, both PVA and PVA/Gel-A nanofibrous hydrogels exhibit a mesoporous structure with average pore diameters of 10.79, 10.75 nm, respectively. Additionally, the adsorption and desorption graphs of PVA and PVA/Gel-A samples in Fig. 5 enable the determining of the adsorption isotherm type for these samples. Generally, adsorption isotherms are classified into six groups by IUPAC,[77] and based on these diagrams and the mesoporous structure of all samples, the type IV isotherm with H4 hysteresis loop can be considered the most suitable isotherm for PVA and PVA/Gel-A (1:1) nanofibers. This type of isotherm is specific to porous compounds, indicating that the substance has very narrow pores in the form of capillaries, leading to a significant increase in absorption. The BET results obtained for PVA nanofibers are in good agreement with the results of other studies.[66,68] As shown in SEM images, PVA nanofibers form random orientations to construct a 3D porous network structure. These random crossover arrangements lead to numerous interconnected voids/porous structures between the fibers, improving the adsorption effect of various substances such as drugs by offering more adsorption sites.[78,79] Furthermore, the nanofibrous hydrogels can offer a large surface area for efficient indicator dye loading and diffusion, ensuring precise and sensitive monitoring of the wound environment. Table 2 summarizes the most important results obtained from BET analysis *e.g.*, surface area, total pore volume, and average pore diameters of pure PVA and PVA/Gel-A (1:1) nanofibers.

Mechanical properties

The compression strength of Gel-A was characterized, revealing a low compression stress (approximately 11 kPa) and compression modulus (approximately 0.19 kPa), as detailed in Table 3. The rheological profile of Gel-A, measured as normal force *versus* gap distance, is shown in Fig. S3. Given that the Young's modulus of soft tissues ranges from 1 to 100 kPa,[80] Gel-A's inherent brittleness, preventing recovery from deformation without fracture, limits its direct application in wound dressing hydrogels. This motivates research into improving the mechanical properties of such hydrogels. To address this limitation, double network PVA/Gel-A nanofibrous hydrogels were investigated in this study. Fig. 6 depicts the tensile strength and elongation at break of PVA and PVA/Gel-A nanofibers as a function of Gel-A concentration. The analysis indicates an optimal PVA/Gel-A ratio of 1:1. This composition exhibited a statistically significant increase in elastic modulus (216%), tensile strength (154.5%), and elongation at break (58%) compared to pristine PVA nanofibers, indicating enhanced mechanical performance relevant to wound dressing applications. The improved mechanical properties are likely due to intermolecular interactions between PVA and Gel-A, leading to network reinforcement and/or enhanced alignment of the Gel-A network within the PVA matrix. Gel-A may function as a reinforcing agent at lower concentrations, increasing matrix stiffness, and as a plasticizer at higher concentrations, enhancing chain mobility.[70,81] In contrast, PVA/Gel-A nanofibers with a higher ratio (1:1.5) showed a reduction in tensile strength (3.98 MPa) and elongation at break (11.72%), potentially resulting from phase separation, reduced structural integrity, or agglomeration. Based on these findings, the PVA/Gel-A (1:1) nanofibrous hydrogel was selected for subsequent experiments, emphasizing the critical role of balanced Gel-A concentration in achieving optimized mechanical properties for targeted applications, thereby defining a specific compositional range for desired attributes. Representative stress–strain curves of PVA/Gel-A nanofibers with varying weight ratios are provided in Fig. S2.

Swelling ratio of nanofibrous hydrogel

Fig. 7a illustrates the swelling behavior of PVA and PVA/Gel-A nanofibrous hydrogels across various pH levels. Both nanofibrous hydrogels exhibit high swelling rates due to their

11630 | *J. Mater. Chem. B*, 2025, **13**, 11621–11639

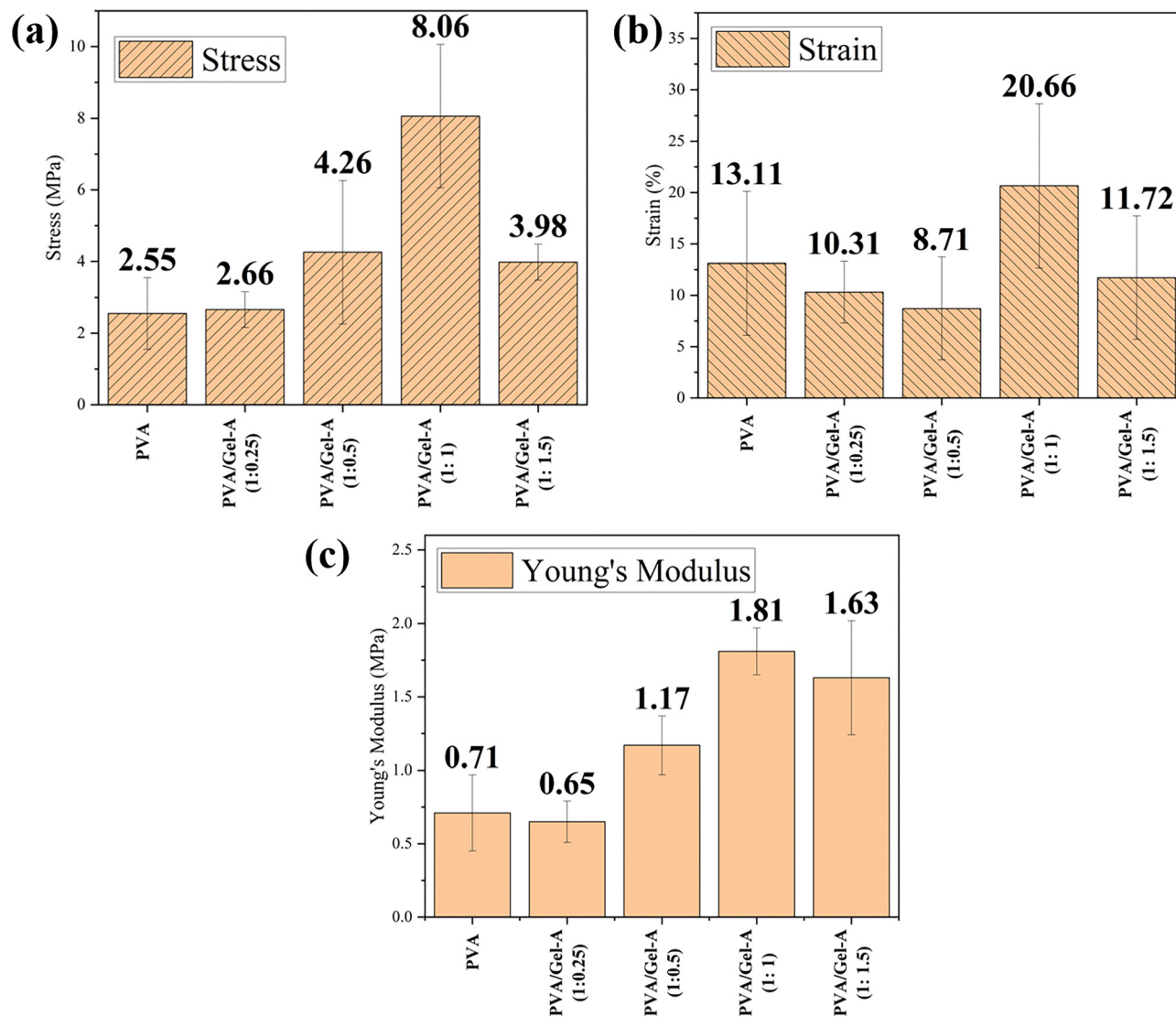This journal is © The Royal Society of Chemistry 2025

Fig. 6 Mechanical properties of PVA/Gel-A nanofibers with varying weight ratios: (a) stress, (b) strain, and (c) Young's modulus. Error bars represent standard deviation ($n = 3$).

hydrophilic nature and nano-porous structure, facilitating fluid absorption and volumetric expansion. This three-dimensional nanostructure enhances water molecule entry.[70,82,83] Maintaining a moist environment, these nanofibrous hydrogels can reduce exudate, retain wound bed moisture, improve collagen matrix, remove cellular debris, and protect the epithelial bed. They can also support blood and nutrient supply, accelerating re-epithelialization.[82]

The swelling rate analysis at different pH levels reveals the anionic nature of PVA hydrogels. Ionization of hydroxyl groups increases the swelling rate with rising pH, with a 136% higher swelling ratio at pH 9 compared to pH 2. Incorporating Gel-A into PVA introduces cationic–anionic characteristics due to amine groups, which ionize under acidic conditions. Previous study indicated pH-responsive behavior of Gel-A, with a maximum swelling ratio of 2500% at pH 1 and deswelling at alkaline pH levels. This was attributed to electrostatic repulsions of protonated amines in acidic environments and partial deprotonation in basic conditions.[51] As shown in Fig. 7A, the swelling ratio of Gel-A was also measured for comparison with PVA and PVA/Gel-A, and the same trend observed in the previous study was obtained.

Moreover, the degradation behavior of PVA and PVA/Gel-A (1:1) in PBS (pH 7.4) over time is illustrated in Fig. S4.

Surface zeta potential

The electric charge of nanofibrous hydrogels was measured at different pH in the range of 3–10 as illustrated in Fig. 7b. As can be seen, the PVA nanofibers exhibited negative ζ-potentials, whereas the ζ-potential of the PVA/Gel-A nanofibers increased to a positive value at acidic pH, reaching approximately +12 mV at pH 3. This shift suggests the presence of amino groups resulting from the successful formation of the Gel-A network on the nanofibers, while pristine PVA nanofibers consistently
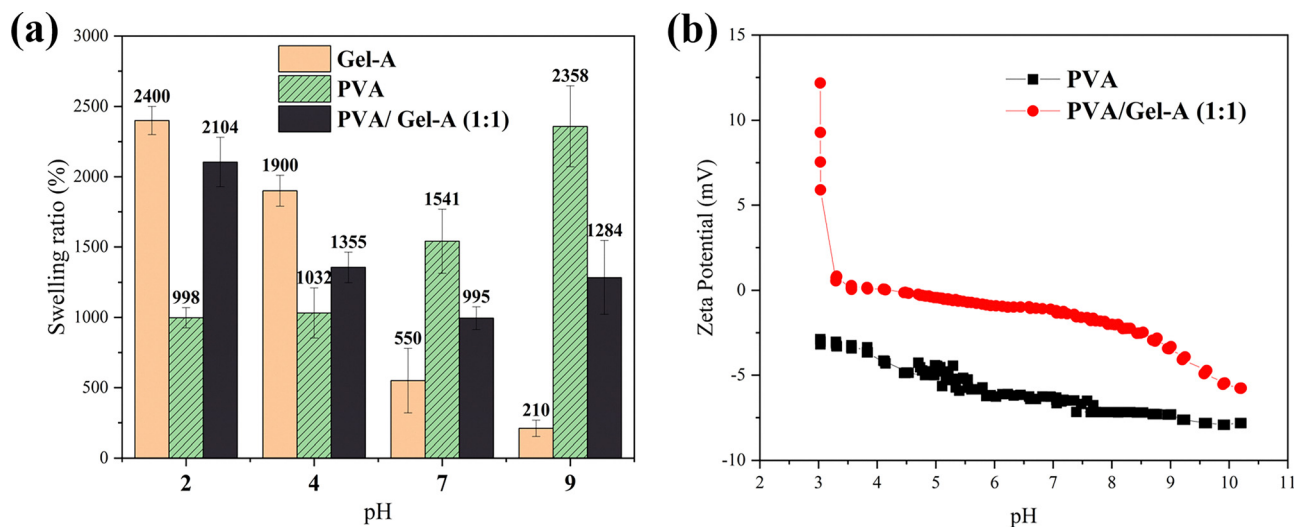
Fig. 7 (a) Swelling ratio of Gel-A, pure PVA, and PVA/Gel-A (1:1) nanofibrous hydrogels as a function of pH after 24 hours of incubation. Error bars represent standard deviation (n = 5). (b) Zeta potential of pure PVA and PVA/Gel-A (1:1) nanofibers as a function of pH.

displayed negative ζ-potentials across all pH levels. The zero point of the ζ-potential (isoelectric point, IEP) was observed at a pH of approximately 4, which aligns closely with the pKa value of 5.35 for the amine group in PP.[84,85] This supported the results of the swelling rate shown in Fig. 7a. Based on the surface ζ-potential and swelling behavior results, a full-IPN PVA/Gel-A nanofibrous hydrogel with coexisting positive and negative surface charges was created. This dual-charged architecture could offer distinct advantages in drug delivery, tissue engineering, and wound healing, including enhanced interactions with charged biomolecules and more controlled drug release profiles.

Importantly, the presence of cationic amine groups, known for their ability to disrupt bacterial membranes, suggests that the hydrogel may possess intrinsic antibacterial activity, although this potential was not the focus of the current study. Such properties could be further exploited in future work by incorporating therapeutic agents or nanoparticles to create a multifunctional platform for both infection monitoring and active treatment. Overall, the cationic–anionic balance in this nanofibrous hydrogel system enhances its versatility, making it a strong candidate for advanced wound care applications.

pH response of halochromic wound dressings

The UV-vis absorption spectra of BTB solution were examined at different pH values. As can be seen in Fig. 8a, the BTB solution was yellow at low pH but turned green with increasing pH and then turned blue at alkaline. The observations indicate that the coloration of the BTB solution is dependent upon the solution's pH. The mechanism of color change is illustrated in the Fig. 8b, which also depict the absorption spectra of the BTB solution. Notably, the UV-vis absorption spectra of BTB solutions at different pH values reveals significant absorption peaks at about 435 nm in acidic conditions and at about 620 nm in basic conditions (Fig. 8c). This color change results from a protonation/deprotonation mechanism which modifies the electron configuration of the BTB, influencing its light
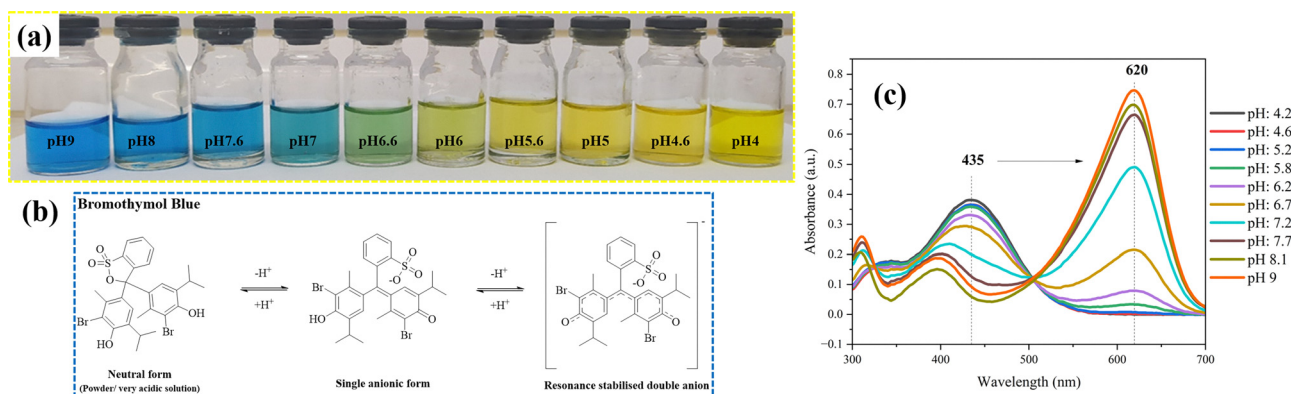

Fig. 8 Bromothymol blue (BTB) as a pH indicator: (a) visual appearance of BTB solutions under varying pH conditions, (b) chemical equilibrium of BTB at acidic and basic pH, and (c) UV-visible absorption spectra of BTB solutions at different pH values.
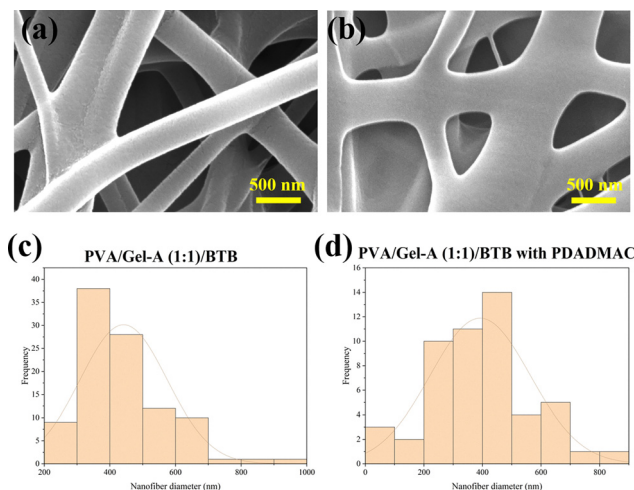
11632 | J. Mater. Chem. B, 2025, **13**, 11621–11639

This journal is © The Royal Society of Chemistry 2025

Fig. 9 SEM images illustrating the morphology of (a) PVA/Gel-A (1:1)/BTB nanofibers and (b) PVA/Gel-A (1:1)/BTB nanofibers complexed with PDADMAC. Histograms displaying the diameter distribution of (c) PVA/Gel-A (1:1)/BTB nanofibers and (d) PVA/Gel-A (1:1)/BTB with PDADMAC.

absorption characteristics.[31] Deprotonation also leads to a ring-opening reaction, reinforcing the role of pH in colorimetric properties of BTB.

As shown in Fig. 9, the encapsulation of BTB within PVA/Gel-A (1:1) nanofibers results in a slightly smaller fiber diameter compared to nanofibers without BTB. Specifically, the average diameter of the BTB-loaded PVA/Gel-A (1:1) nanofibers was 440 ± 130 nm, with a 1:1 ratio of PVA to Gel-A. In contrast, the corresponding PVA/Gel-A (1:1) nanofibers without BTB exhibited an average diameter of 675 ± 136 nm. This suggests that BTB influences the solution's properties, such as viscosity or surface tension, which in turn affects the fiber formation process, leading to a minimal but noticeable reduction in fiber diameter.

The presence of PDADMAC as a complexing agent leads to the formation of fusions between the nanofibers, resulting in an average diameter of 392 ± 171 nm. However, this does not result in a statistically significant increase in diameter compared to the corresponding nanofibers without PDADMAC, suggesting that the primary effect is on fiber morphology rather than size.

The halochromic behavior of PVA/Gel-A (1:1)/BTB nanofibers, both with and without PDADMAC, was investigated to explore their potential use as smart wound dressings that indicate pH changes. This investigation demonstrates their effectiveness in responding to pH changes, a critical factor for halochromic applications in wound care management. As shown in Fig. 10, the incorporation of BTB serves as a pH-sensitive indicator, allowing all nanofibers to exhibit visually distinguishable color changes, from yellow in acidic conditions to green in neutral and blue in alkaline environments. These changes are visible to the naked eye within just 1 minute of response time. This feature could enable clinicians to conduct rapid, non-invasive wound assessments and also could give patients real-time feedback on their healing progress. Fig. 10a

and b present digital photographs illustrating the pH-dependent colorimetric response of PVA/Gel-A (1:1)/BTB nanofibrous hydrogels, both with and without the PDADMAC complexing agent, following exposure to buffer solutions at pH 4, 7, and 9.

According to Table 4, the PVA/Gel-A (1:1)/BTB nanofibers at pH 4 (S1) exhibited high lightness (L^*) and a light-yellow hue, as indicated by the positive a^* and b^* values. The hue angle (h°) of 65.13° further confirms that the color of this sample lies within the yellow-red region of the color wheel.

As the pH increased to 7, the L^* of sample S2 decreased significantly, resulting in a darker coloration with a hue shift toward green, reflected by the negative a^* value. Additionally, the minimal presence of yellow was indicated by a b^* value approaching zero, while the hue angle ($h^\circ = 175.73^\circ$) showed that the sample at pH 7 is located in the second quadrant of the CIELAB color space. This pH adjustment also led to a decrease in chroma (C^* value) compared to S1.
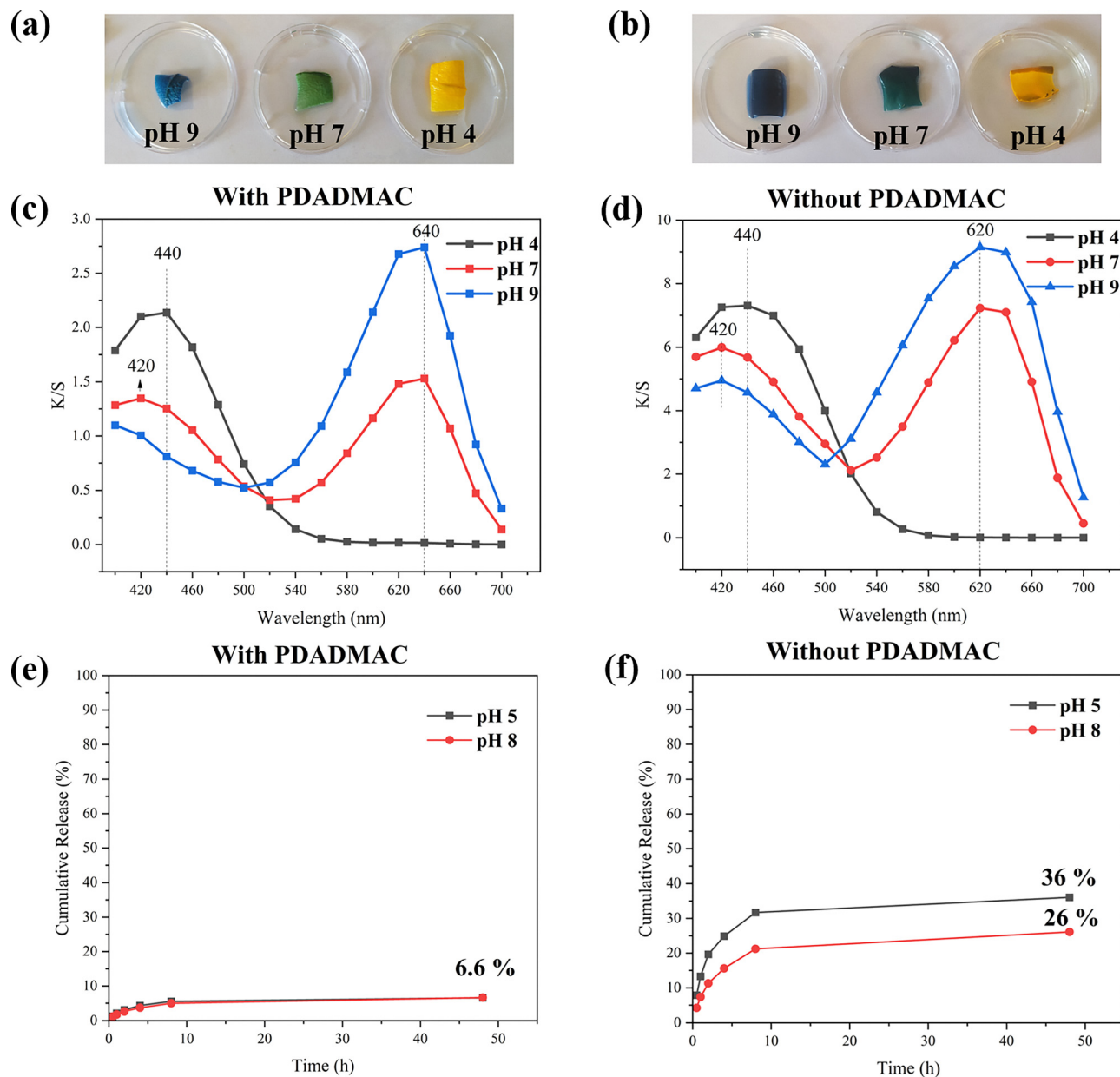
It was found that the nanofiber sample at pH 9 (S3) appeared even darker, with both a^* and b^* values turning negative, suggesting a shift in the color hues of BTB toward a greenish direction on the red-green axis and toward a bluish direction on the yellow-blue axis, respectively. The hue angle ($h^\circ = 195.47^\circ$) also confirmed a shift toward blue-green region of the color space (the third quadrant). Notably, S3 exhibited the lowest C^* value among the samples, indicating the lowest chromatic purity. Overall, these calorimetric data, particularly the hue angle values for the three samples, demonstrate significant and distinguishable color differences between S1, S2, and S3.

In contrast, Table 5 illustrates that the PVA/Gel-A (1:1)/BTB nanofibers incorporating PDADMAC exhibited comparable initial characteristics at pH 4 (S4), demonstrating high lightness and yellow-red hues, with an h° value of 81.99°, along with positive a^* and b^* values. Upon changing the pH to neutral (pH 7), the lightness of sample S5 decreased; however, the color retained a greenish-yellow hue, evidenced by a slight positive b^* value despite a negative a^* value. Additionally, S5 displayed reduced chroma compared to the sample at pH 4, with a hue angle of 153.52°, indicating that the color is situated in the green-yellow region of the CIELAB color space.

At pH 9, the nanofiber sample (S6) manifested a further reduction in L^* and transitioned to a more pronounced greenish-blue hue, as indicated by an h° value of 208.41° and negative a^* and b^* values. Notably, the hue angle changes of the PVA/Gel-A (1:1)/BTB nanofibers containing PDADMAC demonstrate a more pronounced transition across these pH levels compared to the sample without PDADMAC, clearly illustrating a progression from yellow at pH 4 to green at pH 7, and ultimately to green-blue at pH 9.

Both wound dressings displayed strong pH sensitivity, exhibiting distinct and reversible color transitions across various pH levels. These findings underscore the potential of these modified nanofibers as highly effective pH indicators in clinical settings, providing healthcare practitioners and patients with immediate visual feedback on wound status and healing progression.

This journal is © The Royal Society of Chemistry 2025

J. Mater. Chem. B, 2025, **13**, 11621–11639 | **11633**

Fig. 10 pH-dependent optical properties of PVA/Gel-A (1 : 1)/BTB nanofibrous hydrogels: (a) and (b) Corresponding digital photographs illustrating the colorimetric response of nanofibrous hydrogels with and without PDADMAC upon exposure to buffer solutions at pH 4, 7, and 9 (response time <1 min); (c) and (d) Kubelka–Munk spectra (K/S) as a function of wavelength for samples with and without PDADMAC, respectively. (e) and (f) *In vitro* release profiles of BTB from PVA/Gel-A (1 : 1) nanofibrous hydrogels (a) with and (b) without PDADMAC at pH 5.0 and 8.0.

Table 4 CIELAB color space coordinates for PVA/Gel-A (1 : 1)/BTB nanofibrous hydrogels, in the absence of a complexing agent, as a function of pH

Sample	pH	L^*	a^*	b^*	C^*	h°
S1	pH 4	74.26	33.36	72.04	79.38	65.13
S2	pH 7	36.59	−17.45	1.51	17.54	175.73
S3	pH 9	33.24	−11.01	−3.22	11.51	195.47

Table 5 CIELAB color space coordinates for PVA/Gel-A (1 : 1)/BTB nanofibrous hydrogels, in the presence of PDADMAC, as a function of pH

Sample	pH	L^*	a^*	b^*	C^*	h°
S4	pH 4	84.15	7.51	53.09	53.63	81.99
S5	pH 7	65.68	−22.09	11.01	24.69	153.52
S6	pH 9	55.14	−21.89	−11.94	24.98	208.41

To gain further insights into the potential of BTB-encapsulated PVA/Gel-A (1 : 1) substrates for monitoring wound

conditions *via* visual color changes, the K/S values across different wavelengths were analyzed. As illustrated in Fig. 10c, the maximum K/S value occurs at λ_{max} = 440 nm for the sample

without PDADMAC at pH 4 (S1), indicating a robust color intensity in acidic conditions. As the pH increases to 7 and 9, two distinct peaks with the λ_{max} values of 420 nm and 620 nm are observed, with the latter showing a higher K/S value. This shift indicates a transition in the dye's absorption spectrum as the environment becomes more alkaline.

Conversely, the substrate containing PDADMAC exhibited similar trends but showed more significant differences in K/S values across pH levels (Fig. 10d), especially between pH 7 and 9, compared to the substrate without the complexing agent while reducing color intensity at all pH levels.

The halochromic behavior observed in both nanofibrous hydrogels, *i.e.*, BTB-encapsulated PVA/Gel-A (1:1) with and without a complexing agent, highlights their effectiveness in indicating pH changes, an essential feature for wound dressings used to monitor healing. The substrate without PDADMAC demonstrates more vigorous color intensity across all tested pH levels. In contrast, the substrate with PDADMAC offers enhanced stability and sensitivity over a wider pH range, although with reduced intensity. This combination of properties makes both formulations suitable for recognizing infection in wounds.

Bromothymol blue retention in wound dressings

Following visual confirmation of the dressing's colorimetric response, quantitative assessment of dye retention within the nanofibrous matrix during incubation in simulated wound fluid (buffer solution) was conducted. Sustained dye retention is critical for maintaining the long-term functionality of the infection-sensing dressing and minimizing potential interference with the wound microenvironment. As depicted in Fig. 10(e and f), PVA/Gel-A (1:1)/BTB nanofibers without PDADMAC exhibited a cumulative dye release of approximately 36% at pH 5 and 26% at pH 8 after 48 hours, highlighting the need for a strategy to improve dye retention within the nanofiber matrix. In contrast, BTB-functionalized PVA/Gel-A (1:1) nanofibers containing PDADMAC demonstrated significantly

reduced dye release, with values below 7% at both pH levels. These results highlight the effectiveness of PDADMAC in preventing dye leaching from the nanofiber matrix. The observed reduction in dye release can be attributed to the ionic interactions between the cationic PDADMAC and the anionic BTB molecules, whose high electron-withdrawing bromine groups promote durable dye encapsulation, thereby enhancing the longevity of the dressing's colorimetric reporting capabilities.

Cytotoxicity

In vitro biocompatibility assessments were performed using keratinocyte cells to evaluate the cytotoxicity and potential sensitizing effects of PVA, Gel-A, BTB-incorporated Gel-A (2.5% w/w BTB relative to Gel-A), and PVA/Gel-A nanofibrous hydrogels. Cell viability was quantified using the Alamar Blue assay, and sensitization potential was assessed *via* the Luciferase assay, both conducted in accordance with OECD guidelines. As illustrated in Fig. 11a, all tested samples exhibited cell viability exceeding 70%, demonstrating acceptable cytocompatibility and biocompatibility. Gel-A exhibited a marginally lower cell viability compared to other samples, potentially attributable to its cationic nature. This observation aligns with previous reports confirming the non-cytotoxic nature of Gel-A towards fibroblast cells.[51] Notably, while the cytotoxicity of the primary PVA/Gel-A/BTB and PVA/Gel-A/BTB/PDADMAC nanofiber formulations was not directly evaluated, encapsulation of BTB within Gel-A did not elicit a major cytotoxic response. This preliminary finding suggests that the incorporation of BTB into the nanofiber matrix is unlikely to introduce significant cytotoxic effects and supports further investigation of the complete formulations for wound dressing applications. Sensitization potential, as determined by fold induction values, remained below the defined threshold of 1.5 for all assessed samples (Fig. 11b). These findings, indicate the biocompatibility of all hydrogels in regard of skin sensitization.
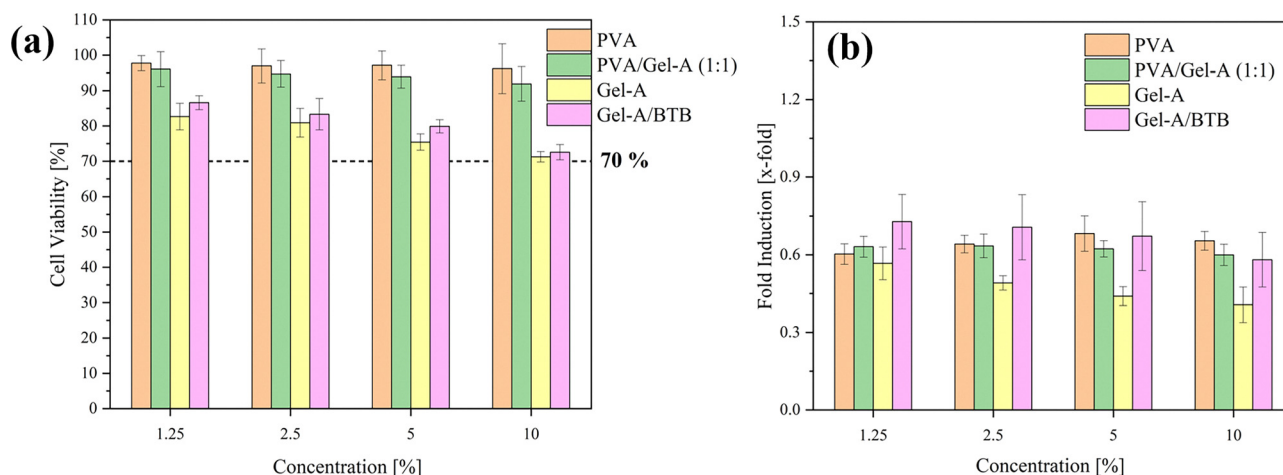
Fig. 11 *In vitro* KeratinoSens skin irritation and sensitization assay including endpoints cell viability (a) and fold induction of a sensitizing response (b) in keratinocyte cells exposed to PVA, PVA/Gel-A (1:1) nanofibers, and Gel-A, with and without BTB incorporation.

This journal is © The Royal Society of Chemistry 2025

J. Mater. Chem. B, 2025, **13**, 11621–11639 | **11635**

Conclusions

The development of pH-sensitive wound dressings capable of real-time infection monitoring represents a significant advancement in modern wound care. In this study, we successfully engineered a nanofibrous hydrogel system based on a IPN comprising PVA and a cationic phosphine-oxide-based hydrogel (Gel-A), with BTB serving as a colorimetric indicator. The novelty of this work lies in the strategic integration of Gel-A and PVA into a mechanically robust and pH-responsive IPN nanofiber system, achieved through a green, dual-function crosslinking process using citric acid and thermal treatment. This approach not only stabilized the PVA matrix but also triggered Gel-A network formation *via* Michael addition chemistry. Additionally, electrospinning was employed to fabricate nanofibrous membranes with a high surface-to-volume ratio, which facilitated efficient dye immobilization and enabled rapid, visible, and reversible colorimetric responses to pH variations, providing a non-invasive and real-time tool for infection monitoring. Importantly, the BTB dye was effectively fixed within the nanofiber matrix, aided by ionic interactions with the cationic network, which prevents dye leaching and minimizes the risk of wound contamination or performance degradation over time. The resulting platform is biocompatible, structurally stable, and scalable, successfully overcoming the key limitations of previously reported hydrogel-based wound sensors. Although the developed nanofibrous hydrogel is not intrinsically adhesive, it is intended to be used alongside commercial adhesive wound dressings, making it compatible with existing clinical applications.

This work lays a promising foundation for the development of dual-functional smart wound dressings. Future research will focus on incorporating antibacterial or therapeutic agents into the hydrogel matrix to enable controlled drug release and enhanced wound healing effects. In addition, *in vitro* antibacterial testing will be conducted to evaluate therapeutic efficacy, followed by further validation through *ex vivo* and *in vivo* wound models to assess infection monitoring and hydrogel performance in biologically relevant environments. Altogether, this platform may offer a versatile and clinically relevant approach to real-time wound monitoring, with promising potential for future therapeutic applications.

Author contributions

Nadia Banitorfi Hoveizavi: conceptualization, methodology, data curation, formal analysis, investigation, writing – original draft, writing – review and editing. Farzaneh Alihosseini: supervision, conceptualization, validation, writing – review and editing. Sandro Lehner: contributed to carry out ICP-OES analysis. Philipp Meier: contributed to carry out cytotoxicity assays. Sabyasachi Gaan: writing – review and editing, and supervision.

Conflicts of interest

There are no conflicts to declare.

Data availability

The data supporting this article have been included in the SI. See DOI: **https://doi.org/10.1039/d5tb01305d**

References

1 R. Dang, J. Xu, B. Zhang, S. Zhao and Y. Dang, Preparation of bacterial cellulose-based antimicrobial materials and their applications in wound dressing: A review, *Mater. Des.*, 2025, 113820.

2 F. Xing, H. Ma, P. Yu, Y. Zhou, R. Luo and Z. Xiang, *et al.*, Multifunctional metal–organic frameworks for wound healing and skin regeneration, *Mater. Des.*, 2023, **233**, 112252.

3 N. Jangra, A. Singla, V. Puri, D. Dheer, H. Chopra and T. Malik, *et al.*, Herbal bioactive-loaded biopolymeric formulations for wound healing applications, *RSC Adv.*, 2025, **15**(16), 12402–12442.

4 L. Sethuram, J. Thomas, A. Mukherjee and N. Chandrasekaran, A review on contemporary nanomaterial-based therapeutics for the treatment of diabetic foot ulcers (DFUs) with special reference to the Indian scenario, *Nanoscale Adv.*, 2022, **4**(11), 2367–2398.

5 N. Xu, Y. Yuan, L. Ding, J. Li, J. Jia and Z. Li, *et al.*, Multifunctional chitosan/gelatin@ tannic acid cryogels decorated with in situ reduced silver nanoparticles for wound healing, *Burns Trauma*, 2022, **10**, tkac019.

6 S. Tan, J. Han, X. Yuan, Z. Song, L. Gao and J. Gao, *et al.*, Epigallocatechin gallate-loaded pH-responsive dressing with effective antioxidant, antibacterial and anti-biofilm properties for wound healing, *Mater. Des.*, 2023, **227**, 111701.

7 Z. Li, Y. Zhao, H. Liu, M. Ren, Z. Wang and X. Wang, *et al.*, pH-responsive hydrogel loaded with insulin as a bioactive dressing for enhancing diabetic wound healing, *Mater. Des.*, 2021, **210**, 110104.

8 Y. Yang, Y. Ren, W. Song, B. Yu and H. Liu, Rational design in functional hydrogels towards biotherapeutics, *Mater. Des.*, 2022, **223**, 111086.

9 M. Salehi, M. Mirhaj, N. B. Hoveizavi, M. Tavakoli and N. Mahheidari, Advancements in Wound Dressings: The Role of Chitin/Chitosan-based Biocomposites, *J. Compos. Compd.*, 2025, **7**, 23.

10 L. A. Wallace, L. Gwynne and T. Jenkins, Challenges and opportunities of pH in chronic wounds, *Ther. Delivery*, 2019, **10**(11), 719–735.

11 Z. Han, M. Yuan, L. Liu, K. Zhang, B. Zhao and B. He, *et al.*, pH-Responsive wound dressings: advances and prospects, *Nanoscale Horiz.*, 2023, **8**(4), 422–440.

12 S. Khattak, I. Ullah, M. Sohail, M. U. Akbar, M. A. Rauf and S. Ullah, *et al.*, Endogenous/exogenous stimuli-responsive smart hydrogels for diabetic wound healing, *Aggregate*, 2025, **6**(2), e688.

13 R. Dong and B. Guo, Smart wound dressings for wound healing, *Nano Today*, 2021, **41**, 101290.

14 T.-H. Kim, S.-C. Kim, W. S. Park, I.-W. Choi, H.-W. Kim and H. W. Kang, *et al.*, PCL/gelatin nanofibers incorporated with starfish polydeoxyribonucleotides for potential wound healing applications, *Mater. Des.*, 2023, **229**, 111912.

15 Q. Pang, F. Yang, Z. Jiang, K. Wu, R. Hou and Y. Zhu, Smart wound dressing for advanced wound management: Real-time monitoring and on-demand treatment, *Mater. Des.*, 2023, **229**, 111917.

16 F. A. Mota, S. A. Pereira, A. R. Araujo, M. L. Passos and M. L. M. Saraiva, Biomarkers in the diagnosis of wounds infection: An analytical perspective, *TrAC, Trends Anal. Chem.*, 2021, **143**, 116405.

17 D. Prakashan, A. Kaushik and S. Gandhi, Smart sensors and wound dressings: Artificial intelligence-supported chronic skin monitoring–A review, *Chem. Eng. J.*, 2024, 154371.

18 K. Wu, X. Wu, M. Chen, H. Wu, Y. Jiao and C. Zhou, H2O2-responsive smart dressing for visible H2O2 monitoring and accelerating wound healing, *Chem. Eng. J.*, 2020, **387**, 124127.

19 Y. Tanaka, L. Sutarlie and X. Su, Detecting bacterial infections in wounds: a review of biosensors and wearable sensors in comparison with conventional laboratory methods, *Analyst*, 2022, **147**(9), 1756–1776.

20 R. Yadav, R. Kumar, M. Kathpalia, B. Ahmed, K. Dua and M. Gulati, *et al.*, Innovative approaches to wound healing: insights into interactive dressings and future directions, *J. Mater. Chem. B*, 2024, **12**(33), 7977–8006.

21 S. O'Callaghan, P. Galvin, C. O'Mahony, Z. Moore and R. Derwin, 'Smart'wound dressings for advanced wound care: a review, *J. Wound Care*, 2020, **29**(7), 394–406.

22 H. Ehtesabi, S.-O. Kalji and L. Movsesian, Smartphone-based wound dressings: a mini-review, *Heliyon.*, 2022, **8**, 7.

23 X. Qiu, F. Xiang, H. Liu, F. Zhan, X. Liu and P. Bu, *et al.*, Electrical hydrogel: electrophysiological-based strategy for wound healing, *Biomater. Sci.*, 2025, **13**(9), 2274–2296.

24 B. Mirani, E. Pagan, B. Currie, M. A. Siddiqui, R. Hosseinzadeh and P. Mostafalu, *et al.*, An advanced multifunctional hydrogel-based dressing for wound monitoring and drug delivery, *Adv. Healthcare Mater.*, 2017, **6**(19), 1700718.

25 A. Tamayol, M. Akbari, Y. Zilberman, M. Comotto, E. Lesha and L. Serex, *et al.*, Flexible pH-sensing hydrogel fibers for epidermal applications, *Adv. Healthcare Mater.*, 2016, **5**(6), 711–719.

26 M. B. Bazbouz and G. Tronci, Two-layer electrospun system enabling wound exudate management and visual infection response, *Sensors*, 2019, **19**(5), 991.

27 L. Van der Schueren and K. De Clerck, Halochromic textile materials as innovative pH-sensors, *Adv. Sci. Technol.*, 2013, **80**, 47–52.

28 E. Soga, M. Akiyama, Y. Ohsaki, W. Hayashi, T. Matsumoto and K. Oana, *et al.*, Isolation of a capnophilic and extended-spectrum β-lactamase-Producing Proteus mirabilis strain from the urine of an octogenarian male patient with acute pyelonephritis, *Jpn. J. Infect. Dis.*, 2019, **72**(3), 193–195.

29 H. Hou, Y. Zhao, C. Li, M. Wang, X. Xu and Y. Jin, Single-cell pH imaging and detection for pH profiling and label-free rapid identification of cancer-cells, *Sci. Rep.*, 2017, **7**(1), 1759.

30 C. Brooker and G. Tronci, A collagen-based theranostic wound dressing with visual, long-lasting infection detection capability, *Int. J. Biol. Macromol.*, 2023, **236**, 123866.

31 T. De Meyer, I. Steyaert, K. Hemelsoet, R. Hoogenboom, V. Van Speybroeck and K. De Clerck, Halochromic properties of sulfonphthaleine dyes in a textile environment: The influence of substituents, *Dyes Pigm.*, 2016, **124**, 249–257.

32 L. Cao, T. Liang, X. Zhang, W. Liu, J. Li and X. Zhan, *et al.*, In-Situ pH-sensitive fibers *via* the anchoring of bromothymol blue on cellulose grafted with hydroxypropyltriethylamine groups *via* adsorption, *Polymers*, 2018, **10**(7), 709.

33 L. Cao, G. Sun, C. Zhang, W. Liu, J. Li and L. Wang, An intelligent film based on cassia gum containing bromothymol blue-anchored cellulose fibers for real-time detection of meat freshness, *J. Agric. Food Chem.*, 2019, **67**(7), 2066–2074.

34 R. Peila, A. Varesano, C. Vineis, V. Bobba, J. Bobba and A. Piriou, *et al.*, Fabric dyeing with colorimetric pH-responsive colours, *Color. Technol.*, 2021, **137**(2), 123–133.

35 Q. Shi, H. Liu, D. Tang, Y. Li, X. Li and F. Xu, Bioactuators based on stimulus-responsive hydrogels and their emerging biomedical applications. NPG Asia, *Materials*, 2019, **11**(1), 64.

36 X. Li, L. Duan, M. Kong, X. Wen, F. Guan and S. Ma, Applications and mechanisms of stimuli-responsive hydrogels in traumatic brain injury, *Gels*, 2022, **8**(8), 482.

37 S. T. Haque, S. K. Saha, M. E. Haque and N. Biswas, Nanotechnology-based therapeutic applications: in vitro and in vivo clinical studies for diabetic wound healing, *Biomater. Sci.*, 2021, **9**(23), 7705–7747.

38 Z. Zheng, H. Zhang, J. Yang, X. Liu, L. Chen and W. Li, *et al.*, Recent advances in structural and functional design of electrospun nanofibers for wound healing, *J. Mater. Chem. B*, 2025, **13**(18), 5226–5263.

39 S.-Q. Chen, Q. Liao, O. W. Meldrum, L. Guo, K. Wang and S. Zhang, *et al.*, Mechanical properties and wound healing potential of bacterial cellulose-xyloglucan-dextran hydrogels, *Carbohydr. Polym.*, 2023, **321**, 121268.

40 W. Zhang, L. Liu, H. Cheng, J. Zhu, X. Li and S. Ye, *et al.*, Hydrogel-based dressings designed to facilitate wound healing, *Mater. Adv.*, 2024, **5**(4), 1364–1394.

41 Y. Hu, L. Yu, Q. Dai, X. Hu and Y. Shen, Multifunctional antibacterial hydrogels for chronic wound management, *Biomater. Sci.*, 2024, **12**, 2460–2479.

42 M. Wang, Z. Deng, Y. Guo and P. Xu, Engineering functional natural polymer-based nanocomposite hydrogels for wound healing, *Nanoscale Adv.*, 2023, **5**(1), 27–45.

43 N. Xu, Y. Gao, Z. Li, Y. Chen, M. Liu and J. Jia, *et al.*, Immunoregulatory hydrogel decorated with Tannic acid/

This journal is © The Royal Society of Chemistry 2025

J. Mater. Chem. B, 2025, **13**, 11621–11639 | **11637**

Ferric ion accelerates diabetic wound healing *via* regulating Macrophage polarization, *Chem. Eng. J.*, 2023, **466**, 143173.

44 D. Rybak, J. Du, P. Nakielski, C. Rinoldi, A. Kosik-Kozioł and A. Zakrzewska, *et al.*, NIR-Light activable 3D printed platform nanoarchitectured with electrospun plasmonic filaments for on demand treatment of infected wounds, *Adv. Healthcare Mater.*, 2025, **14**(6), 2404274.

45 M. Baghali, W. Jayathilaka and S. Ramakrishna, The role of electrospun nanomaterials in the future of energy and environment, *Materials*, 2021, **14**(3), 558.

46 M. He, F. Ou, Y. Wu, X. Sun, X. Chen and H. Li, *et al.*, Smart multi-layer PVA foam/CMC mesh dressing with integrated multi-functions for wound management and infection monitoring, *Mater. Des.*, 2020, **194**, 108913.

47 S. Pourshahrestani, E. Zeimaran and M. B. Fauzi, Antibacterial polylysine-containing hydrogels for hemostatic and wound healing applications: Preparation methods, current advances and future perspectives, *Biomater. Sci.*, 2024, **12**(13), 3293–3320.

48 S. S. Das, D. Sharma, B. V. K. Rao, M. K. Arora, J. Ruokolainen and M. Dhanka, *et al.*, Natural cationic polymer-derived injectable hydrogels for targeted chemotherapy, *Mater. Adv.*, 2023, **4**(23), 6064–6091.

49 B. Borkoyev and K. Saliyeva, *The efficiency of cationic-based hydrogels in heavy metal removal from wastewater*. 2023.

50 G. R. Deen and X. J. Loh, Stimuli-responsive cationic hydrogels in drug delivery applications, *Gels*, 2018, **4**(1), 13.

51 R. Nazir, D. Parida, A. G. Guex, D. Rentsch, A. Zarei and A. Gooneie, *et al.*, Structurally tunable pH-responsive phosphine oxide based gels by facile synthesis strategy, *ACS Appl. Mater. Interfaces*, 2020, **12**(6), 7639–7649.

52 J. Chen, S. Han, M. Huang, J. Li, M. Zhou and J. He, Green crosslinked nanofibers membrane based on CS/PVA combined with polybasic organic acid for tympanic membrane repair, *Int. J. Polym. Mater. Polym. Biomater.*, 2022, **71**(4), 291–301.

53 Chemico I. Test Guideline No. 442C. 2023.

54 *ISO 10993-12. Biological Evaluation of Medical Devices. Part 12: Sample Preparation and Reference Materials; International Organization for Standardization*, Geneva, Switzerland, 2012.

55 N. B. Hoveizavi and M. Feiz, Synthesis of novel dyes containing a dichlorotriazine group and their applications on nylon 6 and wool, *Dyes Pigm.*, 2023, **212**, 111086.

56 M. Alizadeh-Sani, M. Tavassoli, D. J. McClements and H. Hamishehkar, Multifunctional halochromic packaging materials: Saffron petal anthocyanin loaded-chitosan nanofiber/methyl cellulose matrices, *Food Hydrocolloids*, 2021, **111**, 106237.

57 J. Lin, Q. Tang, D. Hu, X. Sun, Q. Li and J. Wu, Electric field sensitivity of conducting hydrogels with interpenetrating polymer network structure, *Colloids Surf., A*, 2009, **346**(1–3), 177–183.

58 S. K. Siddhanta and R. Gangopadhyay, Conducting polymer gel: formation of a novel semi-IPN from polyaniline and crosslinked poly (2-acrylamido-2-methyl propanesulphonicacid), *Polymer*, 2005, **46**(9), 2993–3000.

59 S. Honmute, S. V. Ganachari, R. Bhat, H. Kumar, D. S. Huh and A. Vankataraman, Studies on polyaniline-polyvinyl alcohol (PANI-PVA) interpenetrating polymer network (IPN) thin films, *Int. J. Sci. Res.*, 2012, **1**(2), 102–106.

60 L. Chikh, V. Delhorbe and O. Fichet, Semi-) Interpenetrating polymer networks as fuel cell membranes, *J. Membr. Sci.*, 2011, **368**(1–2), 1–17.

61 R. Nazir, D. Parida, J. Borgstädt, S. Lehner, M. Jovic and D. Rentsch, *et al.*, In-situ phosphine oxide physical networks: A facile strategy to achieve durable flame retardant and antimicrobial treatments of cellulose, *Chem. Eng. J.*, 2021, **417**, 128028.

62 A. Zarei, F. Alihosseini, D. Parida, R. Nazir and S. Gaan, Fabrication of cellulase catalysts immobilized on a nanoscale hybrid polyaniline/cationic hydrogel support for the highly efficient catalytic conversion of cellulose, *ACS Appl. Mater. Interfaces*, 2021, **13**(42), 49816–49827.

63 P. Simonetti, R. Nazir, A. Gooneie, S. Lehner, M. Jovic and K. A. Salmeia, *et al.*, Michael addition in reactive extrusion: A facile sustainable route to developing phosphorus based flame retardant materials, *Composites, Part B*, 2019, **178**, 107470.

64 M. Najafi, J. Chery and M. M. Frey, Functionalized electrospun poly (vinyl alcohol) nanofibrous membranes with poly (methyl vinyl ether-*alt*-maleic anhydride) for protein adsorption, *Materials*, 2018, **11**(6), 1002.

65 A. Doustgani, Optimization of mechanical and structural properties of PVA nanofibers, *J. Ind. Text.*, 2016, **46**(3), 901–913.

66 X. Wang, Q. Fu, X. Wang, Y. Si, J. Yu and X. Wang, *et al.*, In situ cross-linked and highly carboxylated poly (vinyl alcohol) nanofibrous membranes for efficient adsorption of proteins, *J. Mater. Chem. B*, 2015, **3**(36), 7281–7290.

67 B. Yang, J. Wang, L. Kang, X. Gao and K. Zhao, Antibacterial, efficient and sustainable CS/PVA/GA electrospun nanofiber membrane for air filtration, *Mater. Res. Express*, 2022, **9**(12), 125002.

68 A. E. de Oliveira, M. L. Aguiar and V. G. Guerra, Improved filter media with PVA/citric acid/Triton X-100 nanofibers for filtration of nanoparticles from air, *Polym. Bull.*, 2021, **78**(11), 6387–6408.

69 S. Lin, R.-Z. Wang, Y. Yi, Z. Wang, L.-M. Hao and J.-H. Wu, *et al.*, Facile and green fabrication of electrospun poly (vinyl alcohol) nanofibrous mats doped with narrowly dispersed silver nanoparticles, *Int. J. Nanomed.*, 2014, 3937–3947.

70 D. Yu, Y. Y. Feng, J. X. Xu, B. H. Kong, Q. Liu and H. Wang, Fabrication, characterization, and antibacterial properties of citric acid crosslinked PVA electrospun microfibre mats for active food packaging, *Packag. Technol. Sci.*, 2021, **34**(6), 361–370.

71 G. C. D. Mata, M. S. Morais, W. P. D. Oliveira and M. L. Aguiar, Composition effects on the morphology of PVA/chitosan electrospun nanofibers, *Polymers*, 2022, **14**(22), 4856.

72 R. C. Chokwe, T. G. Kebede, S. Dube and M. M. Nindi, Fabrication of electrospun Mondia whitei/PVA nanofibres: application in the removal of acidic drugs, *Heliyon.*, 2022, **8**, 10.

11638 | *J. Mater. Chem. B*, 2025, **13**, 11621–11639

This journal is © The Royal Society of Chemistry 2025

73 A. Suratman, D. N. Astuti, R. Jonathan, A. Kuncaka and Y. Yusuf, Fabrication of Alginate-Based Electrospun Nanofibers for Carbon Dioxide Removal, *Indones. J. Chem.*, 2022, **22**(2), 317–330.

74 F. Rahmani, H. Ziyadi, M. Baghali, H. Luo and S. Ramakrishna, Electrospun PVP/PVA nanofiber mat as a novel potential transdermal drug-delivery system for buprenorphine: a solution needed for pain management, *Appl. Sci.*, 2021, **11**(6), 2779.

75 E. P. F. Nhavene, G. F. Andrade, J. A. Q. A. Faria, D. A. Gomes and E. M. B. D. Sousa, Biodegradable polymers grafted onto multifunctional mesoporous silica nanoparticles for gene delivery, *Chem. Eng.*, 2018, **2**(2), 24.

76 G. G. Lara, M. F. Cipreste, G. F. Andrade, W. M. D. Silva and E. M. B. D. Sousa, Response of Fibroblasts MRC-5 to Flufenamic Acid-Grafted MCM-41 Nanoparticles, *Bioengineering.*, 2018, **5**(1), 4.

77 M. Thommes, K. Kaneko, A. V. Neimark, J. P. Olivier, F. Rodriguez-Reinoso and J. Rouquerol, *et al.*, Physisorption of gases, with special reference to the evaluation of surface area and pore size distribution (IUPAC Technical Report), *Pure Appl. Chem.*, 2015, **87**(9–10), 1051–1069.

78 Y. Yang, Z. Zhang, M. Wan, Z. Wang, X. Zou and Y. Zhao, *et al.*, A facile method for the fabrication of silver nanoparticles surface decorated polyvinyl alcohol electrospun nanofibers and controllable antibacterial activities, *Polymers*, 2020, **12**(11), 2486.

79 J. C. Ge, G. Wu, S. K. Yoon, M. S. Kim and N. J. Choi, Study on the preparation and lipophilic properties of polyvinyl alcohol (PVA) nanofiber membranes *via* green electrospinning, *Nanomaterials*, 2021, **11**(10), 2514.

80 Y. Yu, H. Yuk, G. A. Parada, Y. Wu, X. Liu and C. S. Nabzdyk, *et al.*, Multifunctional "hydrogel skins" on diverse polymers with arbitrary shapes, *Adv. Mater.*, 2019, **31**(7), 1807101.

81 M. Eichers, D. Bajwa, J. Shojaeiarani and S. Bajwa, Biobased plasticizer and cellulose nanocrystals improve mechanical properties of polylactic acid composites, *Ind. Crops Prod.*, 2022, **183**, 114981.

82 N. Shankhwar, M. Kumar, B. B. Mandal, P. Robi and A. Srinivasan, Electrospun polyvinyl alcohol-polyvinyl pyrrolidone nanofibrous membranes for interactive wound dressing application, *J. Biomater. Sci., Polym. Ed.*, 2016, **27**(3), 247–262.

83 H. Morad, M. Jahanshahi, J. Akbari, M. Saeedi, P. Gill and R. Enayatifard, Formulation, optimization and evaluation of nanofiber based fast dissolving drug delivery system of colchicine for pediatrics, *J. Pediatr. Perspect.*, 2021, **9**(3), 13213–13224.

84 R. Kant and S. Maji, Recent advances in the synthesis of piperazine based ligands and metal complexes and their applications, *Dalton Trans.*, 2021, **50**(3), 785–800.

85 J. Desantis, A. Mammoli, M. Eleuteri, A. Coletti, F. Croci and A. Macchiarulo, *et al.*, PROTACs bearing piperazine-containing linkers: what effect on their protonation state?, *RSC Adv.*, 2022, **12**(34), 21968–21977.

This journal is © The Royal Society of Chemistry 2025

J. Mater. Chem. B, 2025, **13**, 11621–11639 | **11639**